

SHARE

RESEARCH ARTICLE



0



0

## Substantial convection and precipitation enhancements by ultrafine aerosol particles

Jiwen Fan<sup>1,\*</sup>, Daniel Rosenfeld<sup>2</sup>, Yuwei Zhang<sup>1,3</sup>, Scott E. Giangrande<sup>4</sup>, Zhanqing Li<sup>3,5</sup>, Luiz A. T. Machado<sup>6</sup>, Scot T. Martin<sup>7</sup>, ...

+ See all authors and affiliations

Science 26 Jan 2018:  
Vol. 359, Issue 6374, pp. 411-418  
DOI: 10.1126/science.aan8461

Article

Figures & Data

Info & Metrics

eLetters

PDF

You are currently viewing the abstract.

[View Full Text](#)



Henrique Barbosa  
Journal Club LFA  
9/Maio/2018

# Abstract

1. Aerosol-cloud interactions remain the largest uncertainty in climate projections.
2. Ultrafine aerosol particles smaller than 50 nanometers (UAP<50) can be abundant in the troposphere but are conventionally considered too small to affect cloud formation.
3. Observational evidence and numerical simulations of deep convective clouds (DCCs) over the Amazon show that DCCs forming in a low-aerosol environment can develop very large vapor supersaturation because fast droplet coalescence reduces integrated droplet surface area and subsequent condensation.
4. UAP<50 from pollution plumes that are ingested into such clouds can be activated to form additional cloud droplets on which excess supersaturation condenses and forms additional cloud water and latent heating, thus intensifying convective strength.
5. This mechanism suggests a strong anthropogenic invigoration of DCCs in previously pristine regions of the world.

● Ultrafine aerosol particles (UAP<sub><50</sub>)

● Cloud droplets from CCN<sub>>50</sub>

● CCN-size aerosol particles (CCN<sub>>50</sub>)

● Cloud droplets from UAP<sub><50</sub>

● Rain drop

● Ice crystal

● Graupel

High

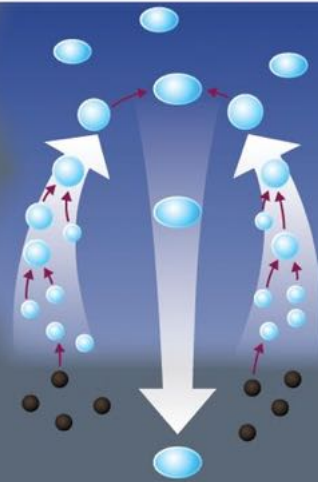


Low

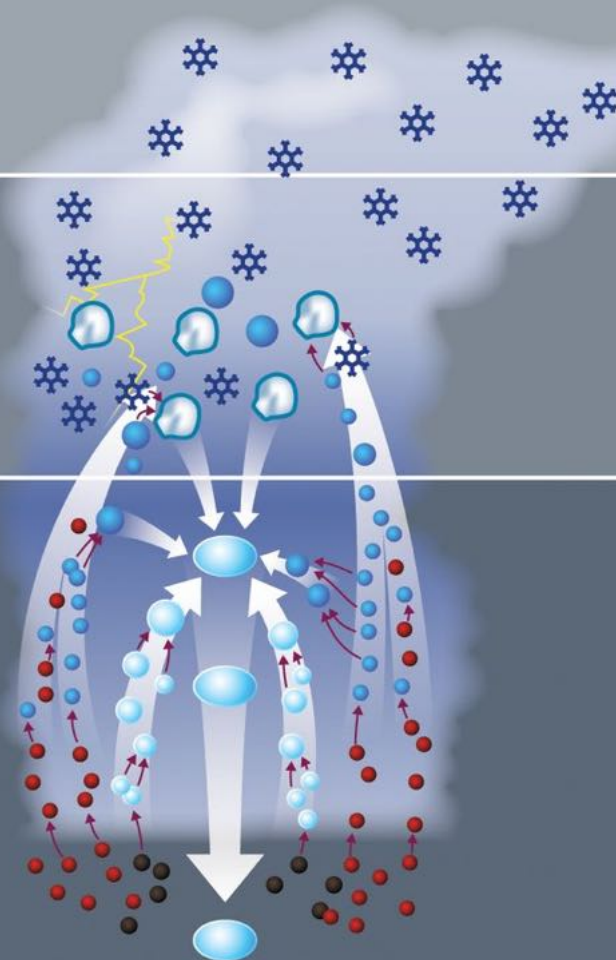
Water supersaturation

-38° C

0° C



CCN<sub>>50</sub>



CCN<sub>>50</sub> + UAP<sub><50</sub>

# Invigoration

- “Previous studies have shown that aerosols could invigorate or suppress DCC intensity through aerosol indirect effects, contingent on dynamical and thermodynamical conditions. “

# Relationships between cloud properties and aerosol loading in Amazonia

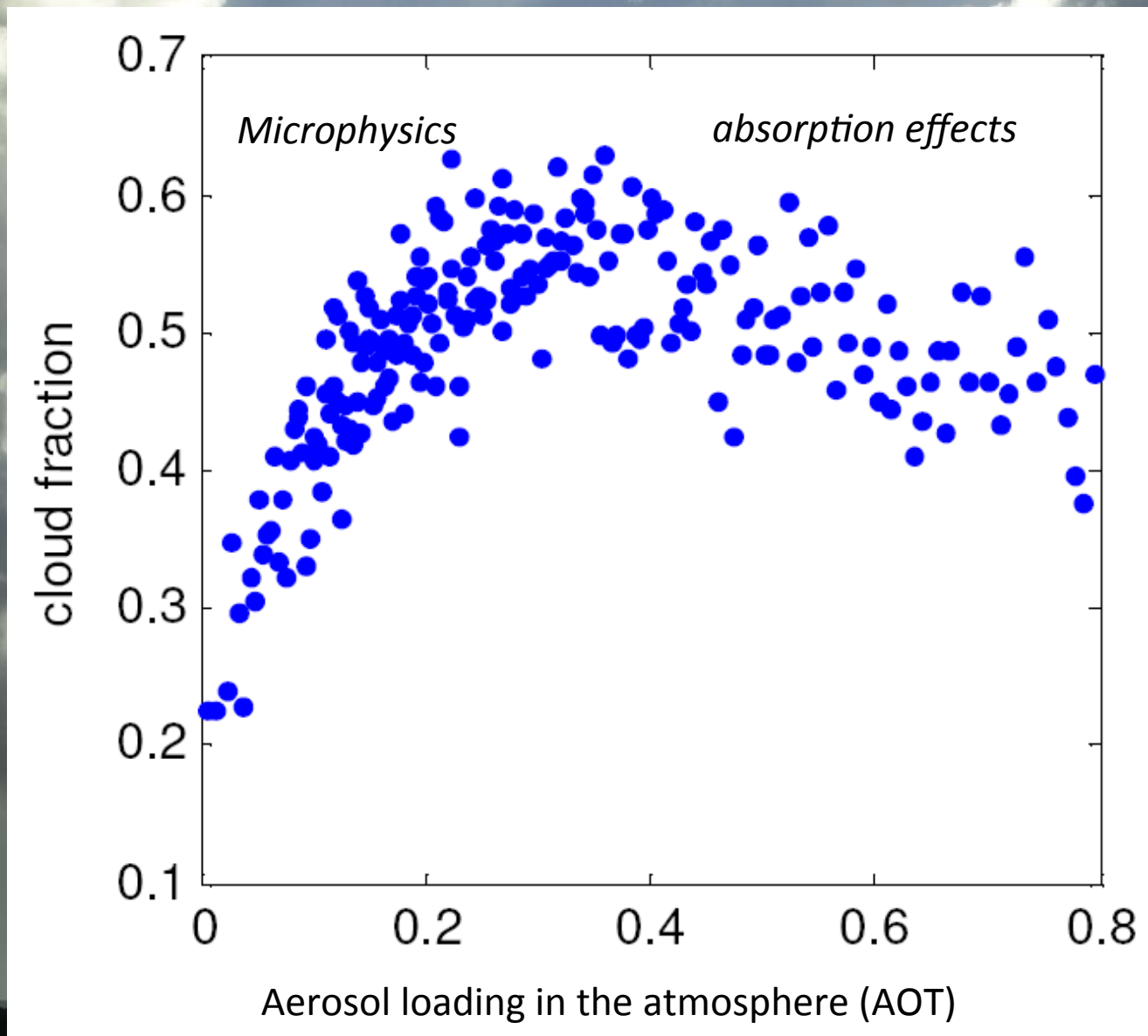




Photo: Ilan Koren



# Terra and Aqua satellite images of the east Amazon basin, 11 August 2002. *(From Koren et al., 2004)*

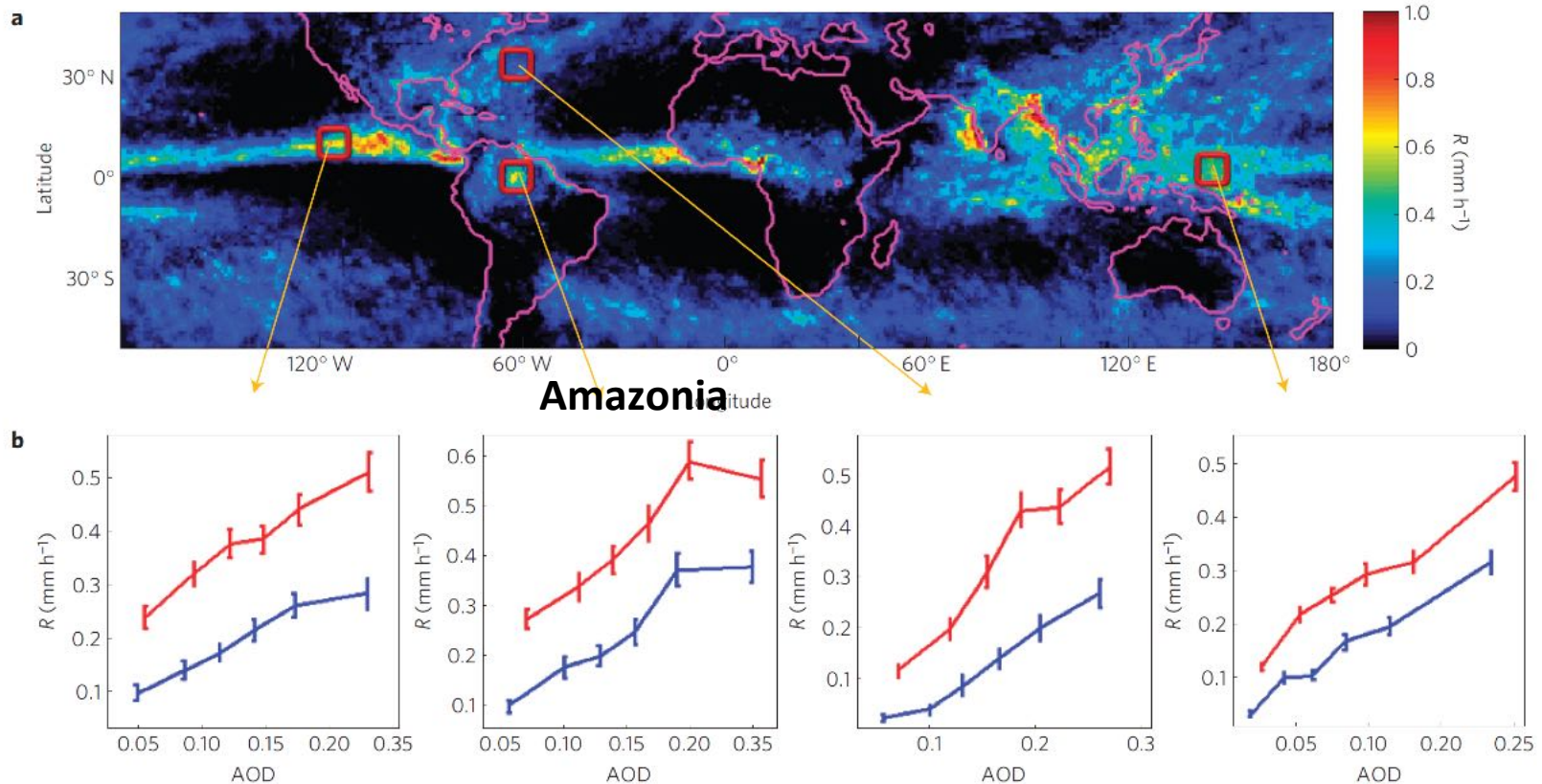
Large scale low cloud suppression



# Rain rate (TRMM) versus Optical Depth (MODIS)

NATURE GEOSCIENCE DOI:10.1038/NCEO1364

LETTERS

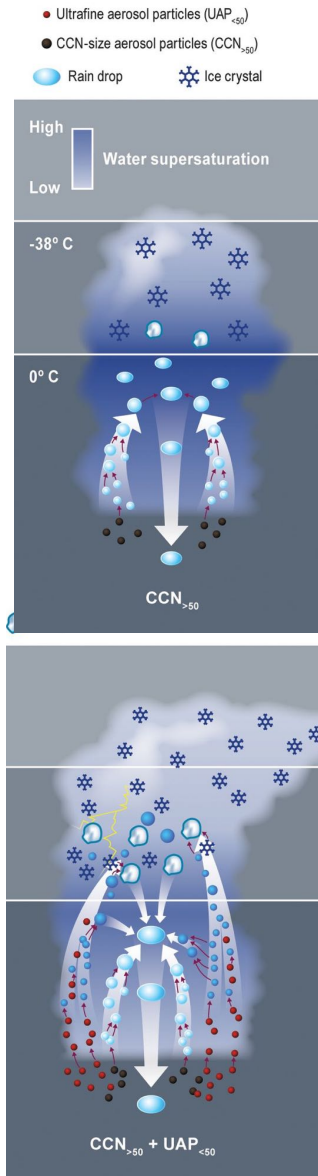


13:30 local-time map of rain rate ( $R$ ) and the observed trend with aerosol loading in four selected regions. Period: July and August 2007. **b**, The average  $R$  values are plotted for six aerosol-loading sets (blue, including zero  $R$  grid squares; red, without zero  $R$  grid squares). Note the  $R$  intensification as a function of AOD in all cases. (Koren et al., Nature 2012)

# Invigoration (cont.)

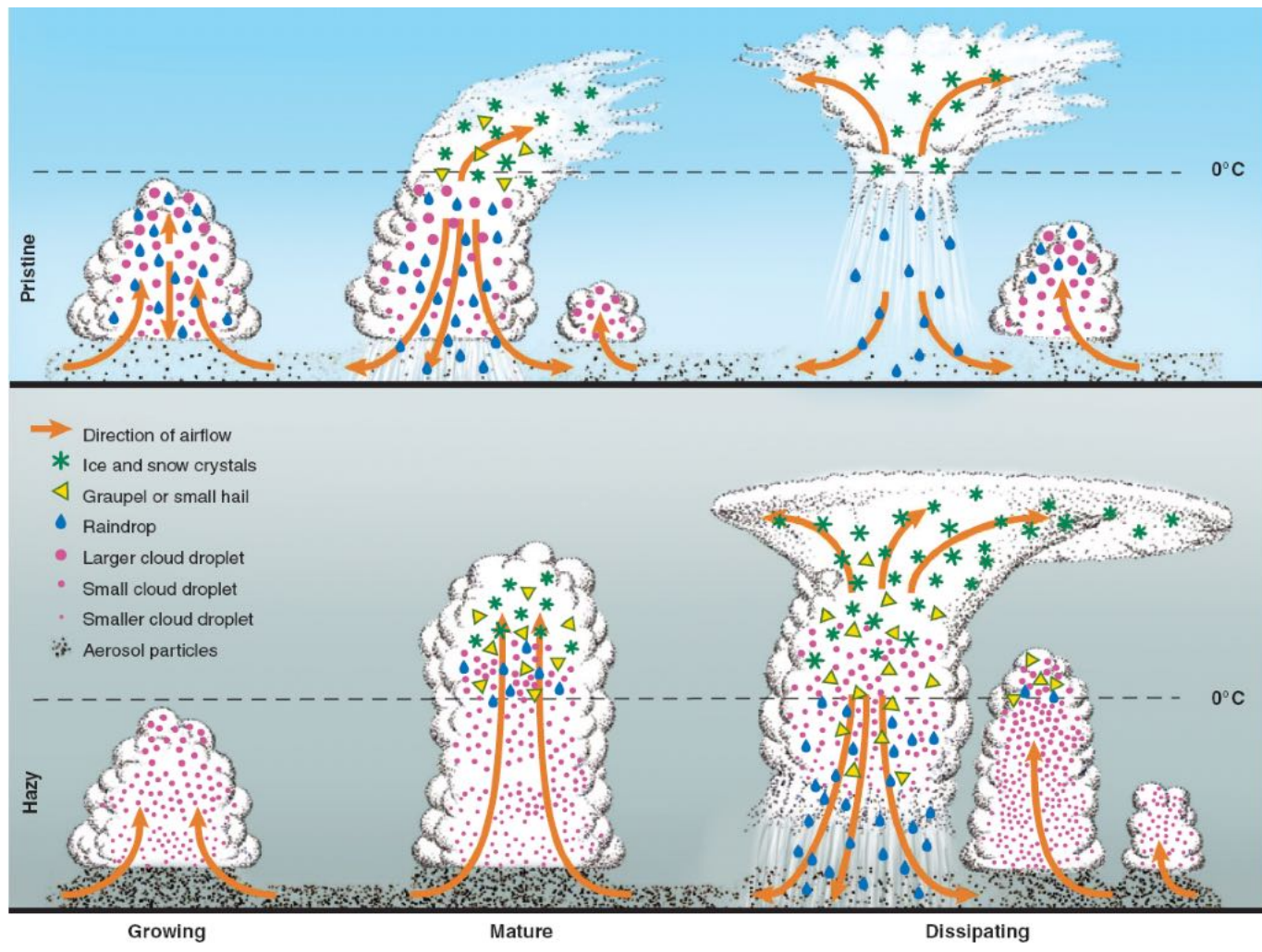
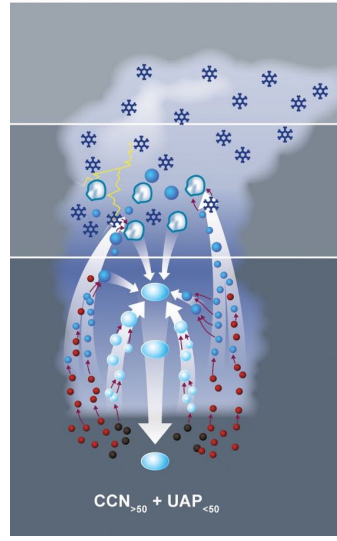
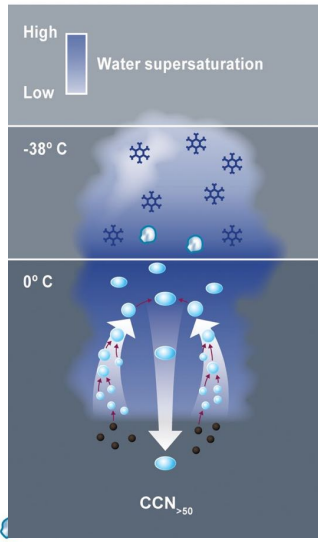
- “In the case of warm-cloud bases ( $>15^{\circ}\text{C}$ ), increasing aerosol concentrations can suppress warm rain because of a reduction in droplet size, which allows more cloud water to be lifted to a higher altitude; “
- “The freezing of this larger amount of cloud water releases additional latent heat, thereby invigorating convective updrafts [referred to as “cold-phase invigoration”]. “
- “Enhancement in DCC intensity favors enhanced storm electrification, larger precipitation rates, and taller clouds with larger anvils. “

# Different process...



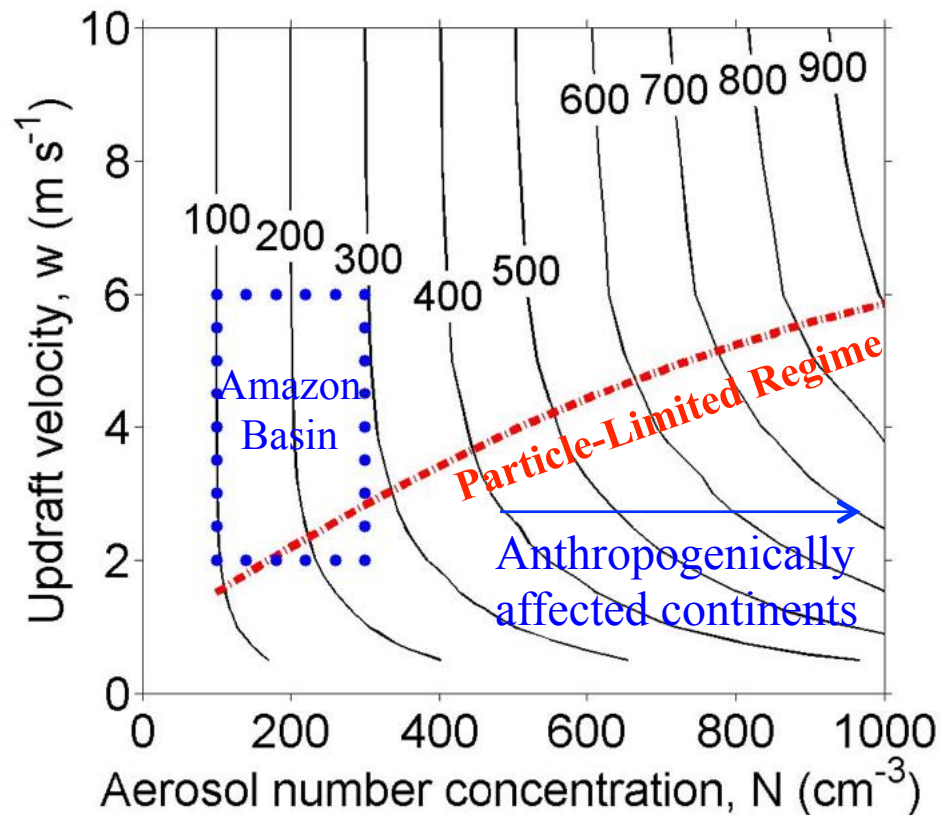
the detailed spectral-bin microphysics scheme to scrutinize the mechanism. We found that the  $\text{UAP}_{<50}$  introduced by the Manaus pollution plume enhanced convective intensity and precipitation rates to a degree not previously observed or simulated. The detailed simulations show that the drastic enhancement in convective intensity is primarily attributable to the enhanced condensational heating, with the latent heat released from enhanced ice-related processes at upper levels playing a secondary role. This differs from the previous “cold-cloud invigoration” concept (13), which does not consider aerosol impacts on condensational heating. As illustrated in Fig. 1, the enhanced condensational heating is driven mainly by the activation of  $\text{UAP}_{<50}$  well above the cloud

- Ultrafine aerosol particles (UAP<sub><50</sub>)
- CCN-size aerosol particles (CCN<sub>>50</sub>)
- Rain drop
- Ice crystal

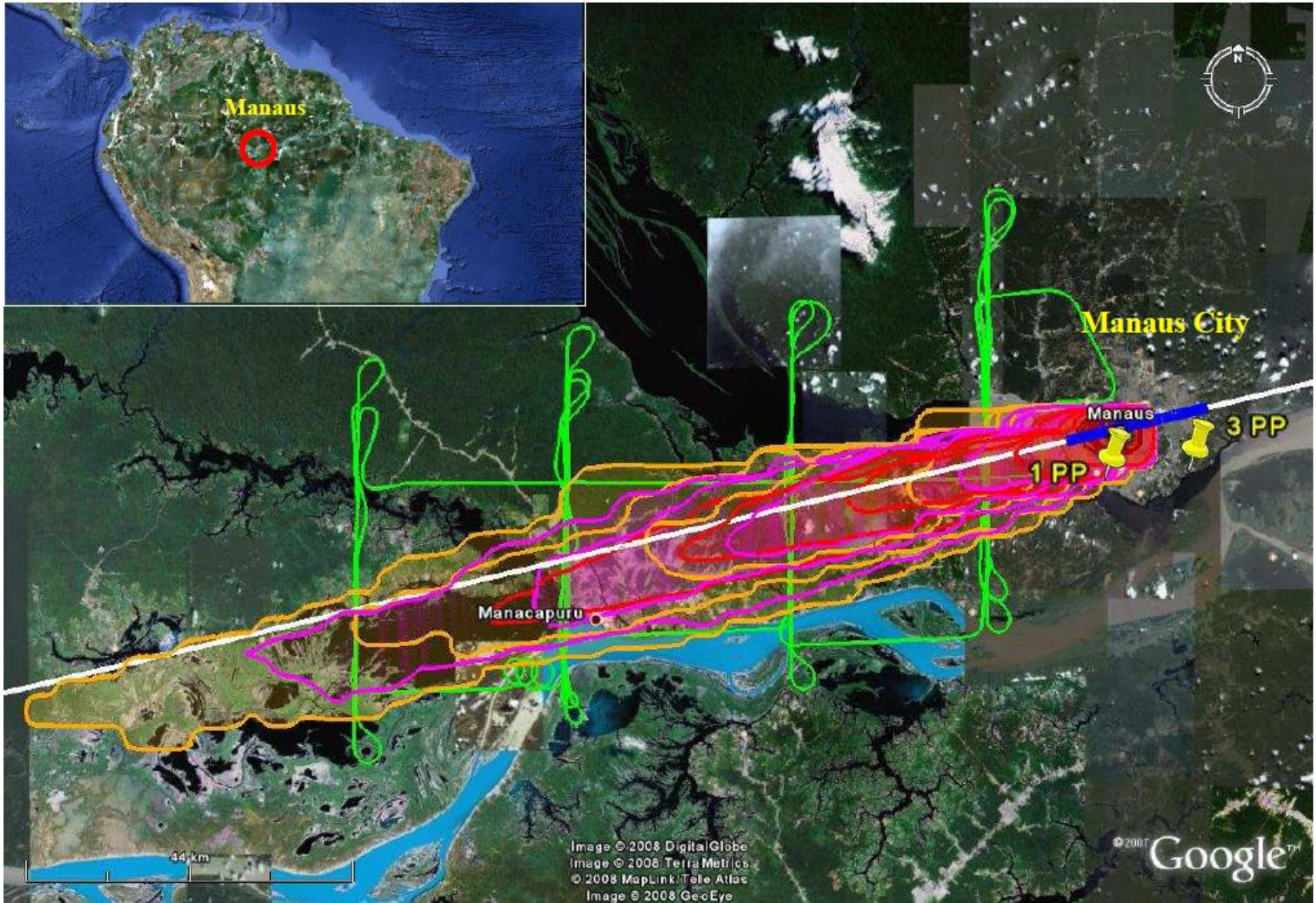


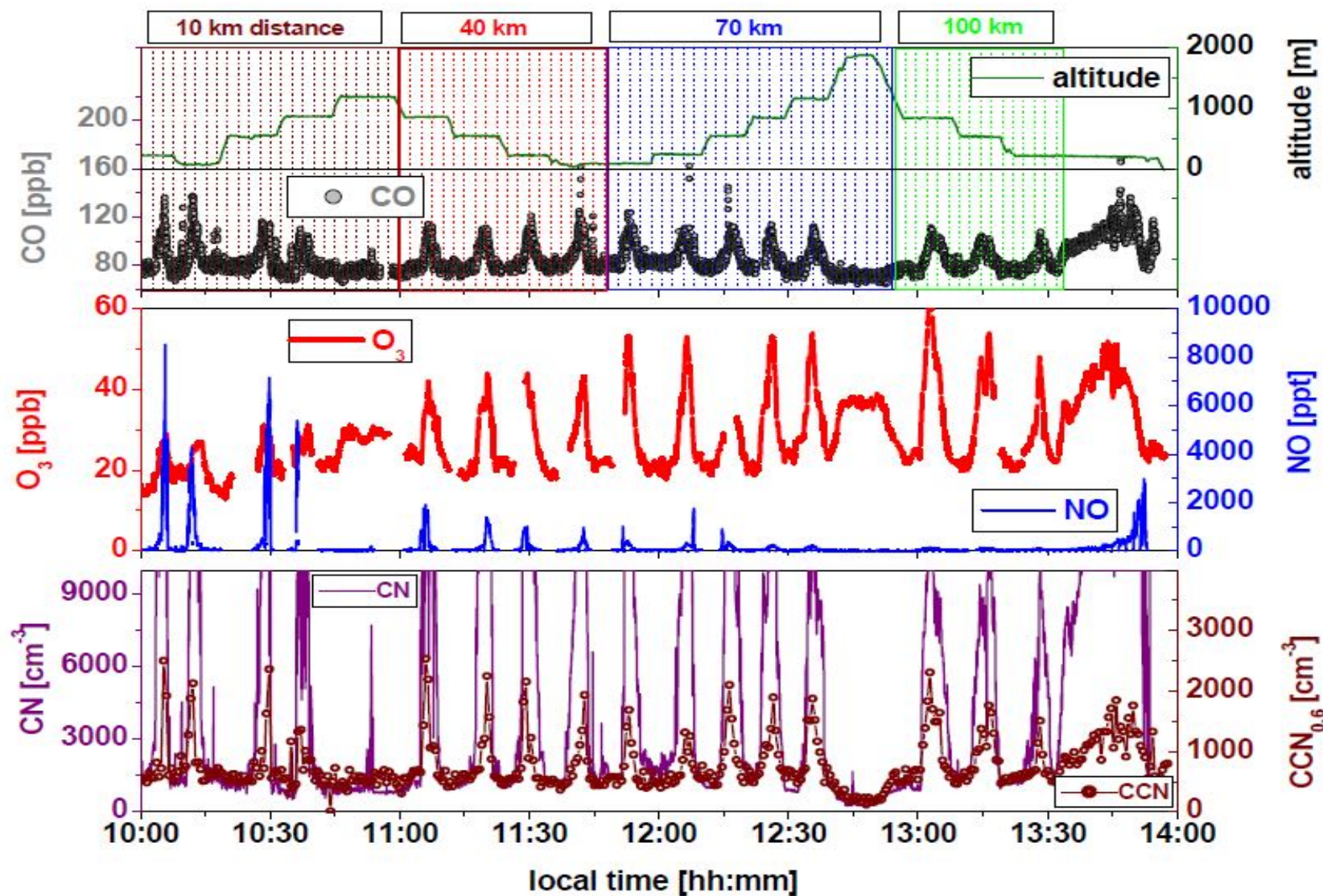
# Why different?

Cloud droplets number concentration



# Experimento GoAmazon 2014/5



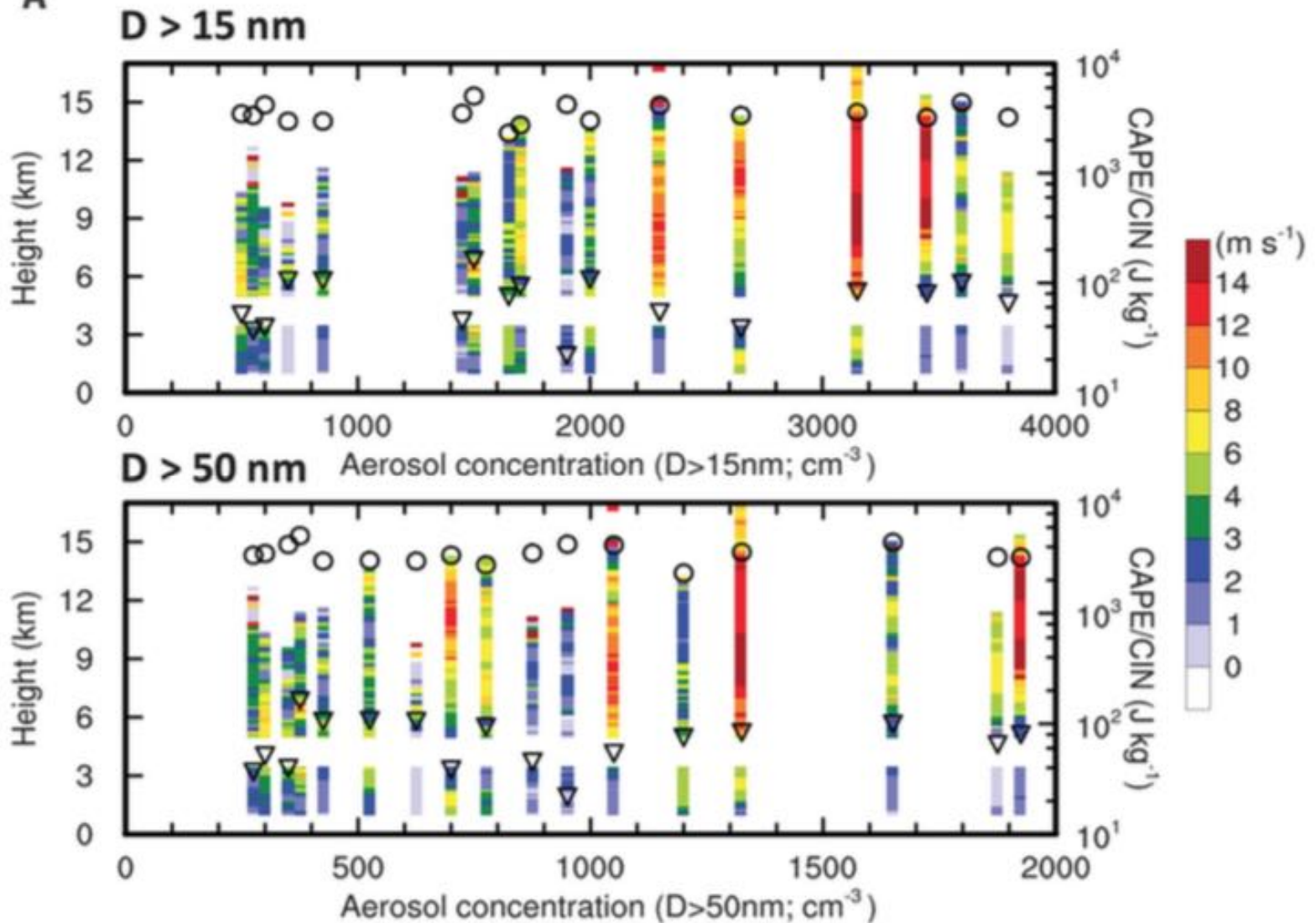


Reference: Kuhn, U.; Ganzeveld, L.; Thielmann, A.; Dindorf, T.; Welling, M.; Sciare, J.; Roberts, G.; Meixner, F. X.; Kesselmeier, J.; Lelieveld, J.; Ciccioli, P.; Kolle, O.; Lloyd, J.; Trentmann, J.; Artaxo, P.; Andreae, M. O., "Impact of Manaus City on the Amazon Green Ocean atmosphere: Ozone production, precursor sensitivity, and aerosol load," *Atmos. Chem. Phys.* **2010**, *10*, 9251-9282.

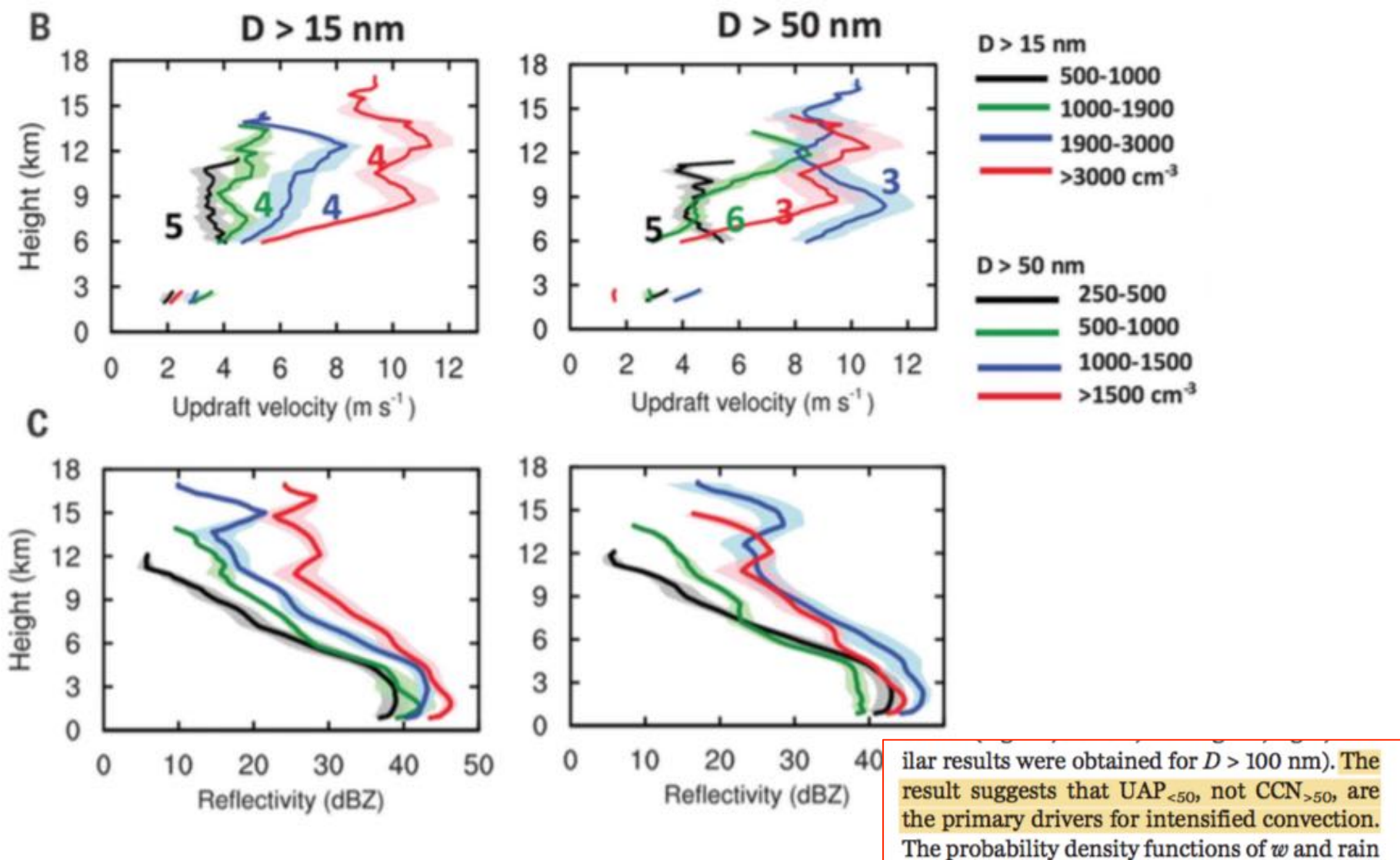
# Method

- DOE/ARM 1290-MHz Ultra High Frequency (UHF) Radar Wind Profilers
- Focused on convective cells of local origin, favoring relatively simple and similar dynamics
- Manaus plume provides aerosol variability
- Our analysis period was the 2014 wet season (1 March to 31 May).

A

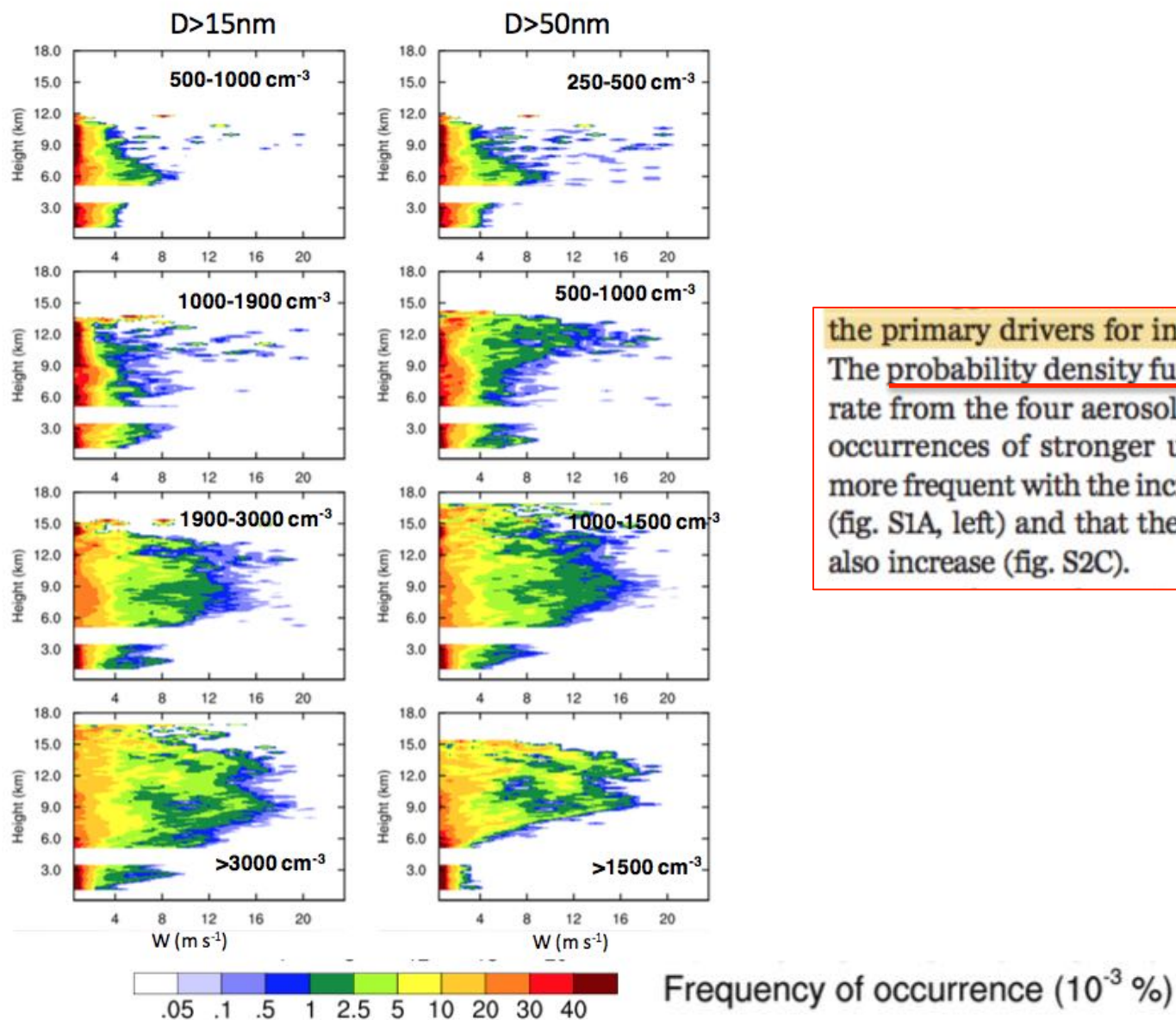


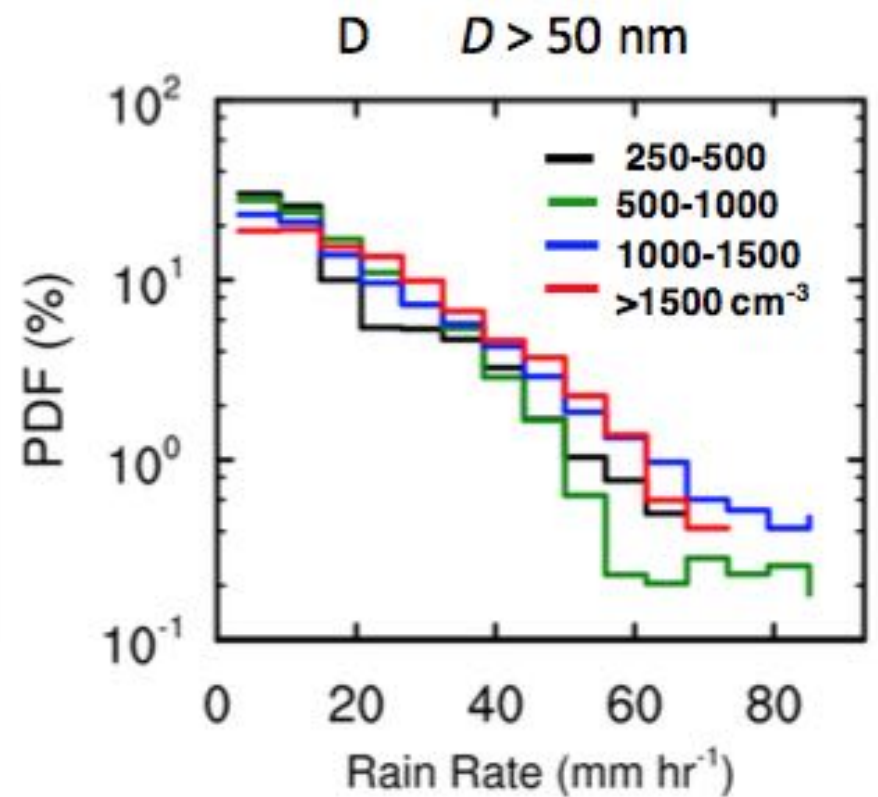
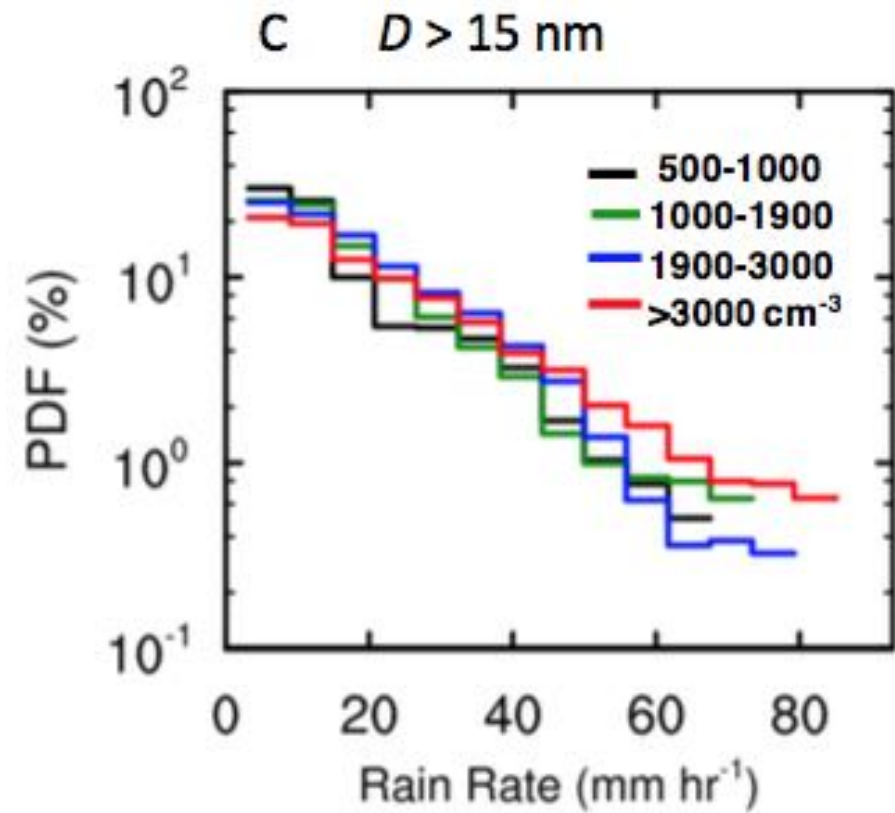
- Mean vertical velocity ( $>p_{90}$ ) of updrafts in each event
- Aerosol particle number concentration (30min before start of convection)



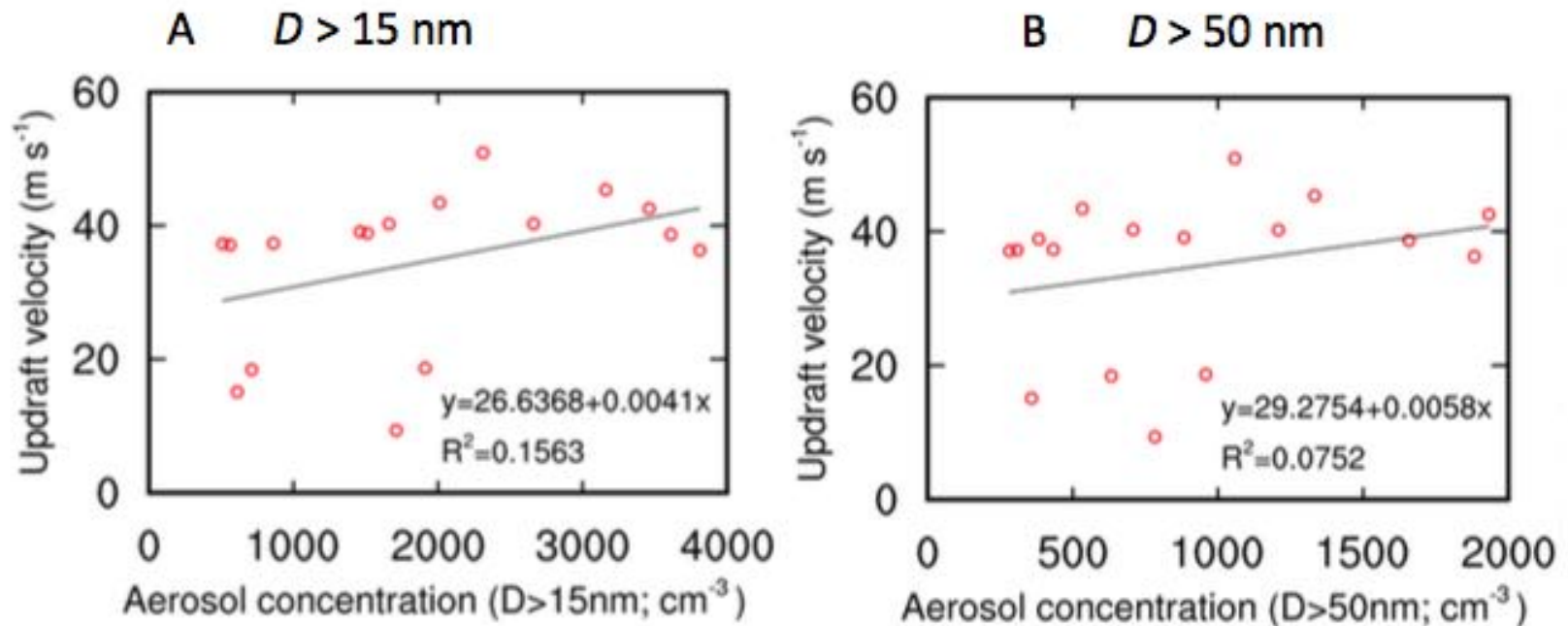
- We found that convective updraft velocity ( $w$ ) increased with an increase of  $N_a$  for aerosols with a diameter ( $D$ ) larger than 15 nm.
- Remarkably, the increasing trend in updraft intensity and radar reflectivity as  $N_a$  increases does not hold well when considering only those aerosols with  $D > 50$  nm

Fig. S1. Vertical profile of PDF of the updraft speeds ( $w$ ;  $\text{m s}^{-1}$ ) in convective area for  $D > 15 \text{ nm}$  (left) and  $D > 50 \text{ nm}$  (right) for the four aerosol groups as in Fig. 2B. For each aerosol group, the frequency for  $w$  in each bin is calculated using an interval of  $1 \text{ m s}^{-1}$  with the number of points divided by the total convective points of the group (i.e., sum of the convective points from the cases of the group).





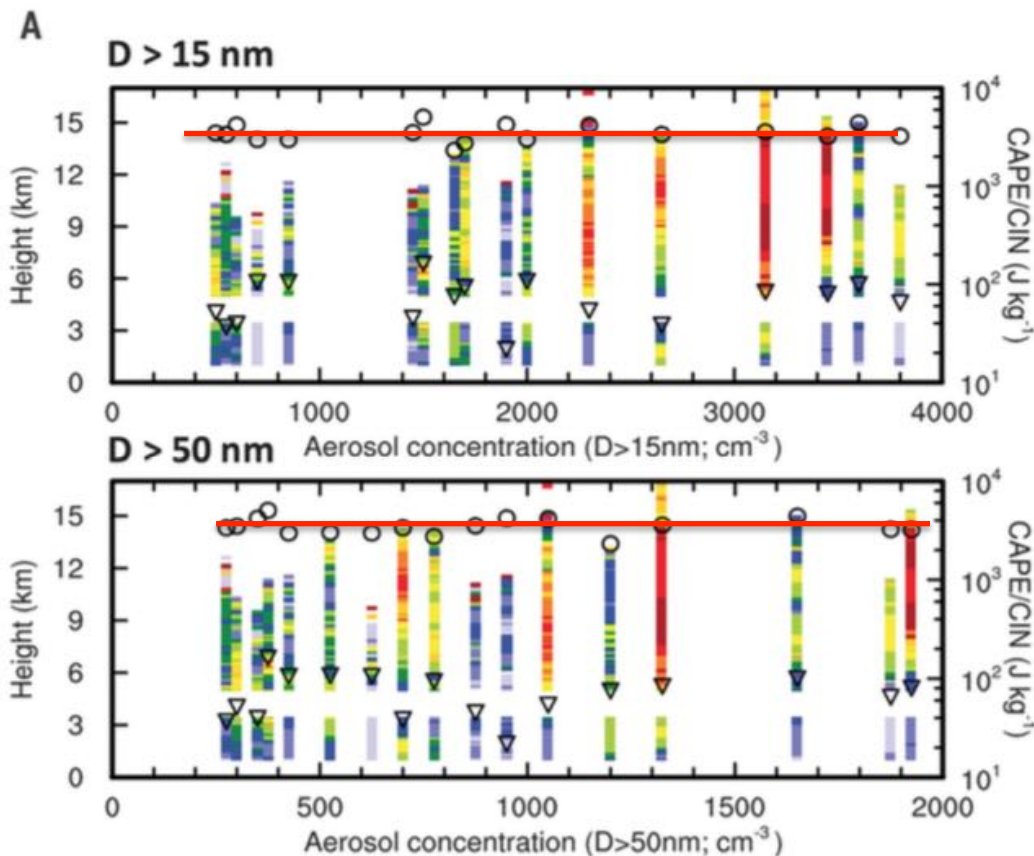
the primary drivers for intensified convection. The probability density functions of  $w$  and rain rate from the four aerosol groups indicate that occurrences of stronger updraft velocities are more frequent with the increase of  $N_a$  for  $\text{UAP}_{<50}$  (fig. S1A, left) and that the maximum rain rates also increase (fig. S2C).

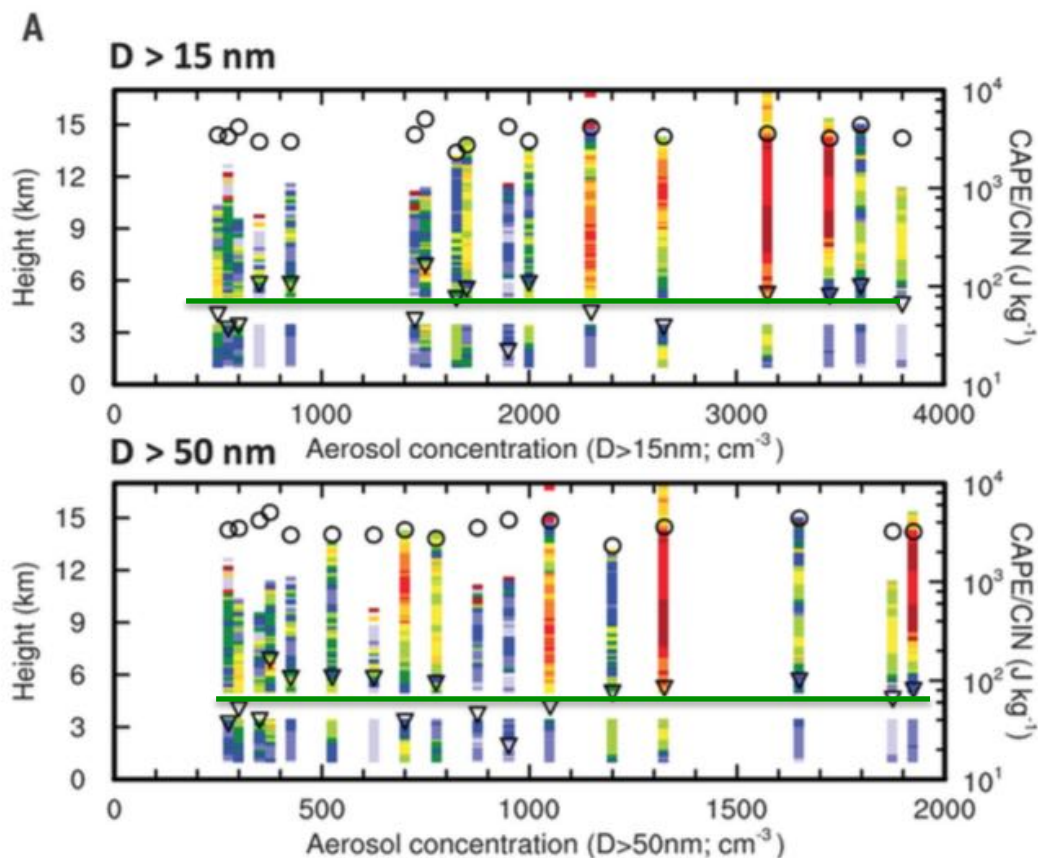


- “Fig. S2. Correlation of the maximum velocity averaged over the top 10 percentiles of updrafts in each case with aerosol concentrations for (A)  $D > 15 \text{ nm}$  and (B)  $D > 50 \text{ nm}$ . (A) shows R2 is doubled for aerosols with  $D > 15 \text{ nm}$  compared with that with  $D > 50 \text{ nm}$ , indicating that the correlation is higher for  $D > 15 \text{ nm}$ . However, the correlation for both  $D > 15 \text{ nm}$  and  $D > 50 \text{ nm}$  are not good because the data are too scattered and the single maximum of vertical velocity may not be representative of convective intensity.”

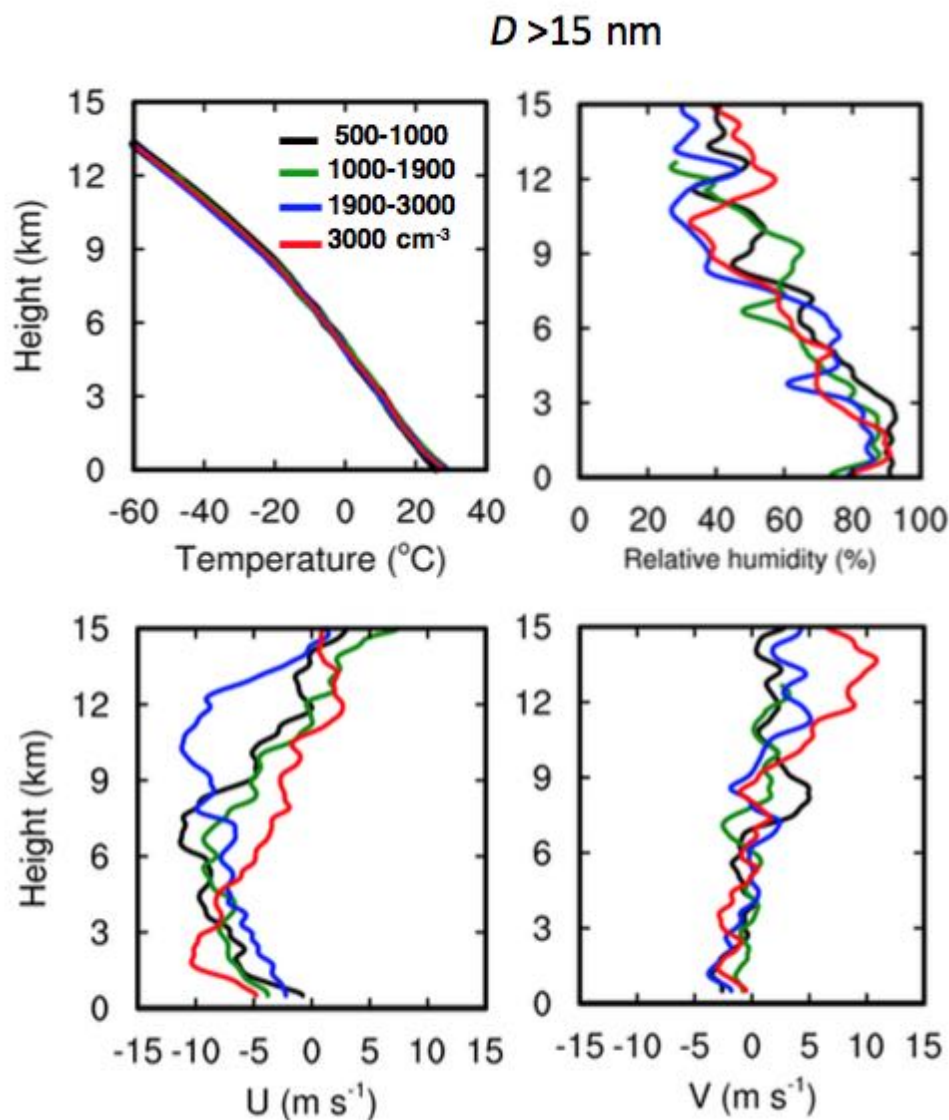
To corroborate that  $UAP_{<50}$  are the main factor contributing to the observed DCC enhancements, we conducted additional analyses to help isolate aerosol effects from thermodynamic controls. Locally driven Amazon deep convective events within the wet season should initiate and evolve under similar diurnal controls on their dynamical and thermodynamical environments (33, 35). We

and thermodynamical environments (33, 35). We examined traditional radiosonde thermodynamic forcing parameters such as the convective available potential energy (CAPE) and convective inhibition (CIN) before convection. The CAPE is very similar for these events (Fig. 2A, black circles) and is not strongly correlated with updraft intensity. Under similar CAPE conditions, CIN magnitudes should help to reveal how likely it is for DCCs to initiate and to determine what may be their relative intensities. CIN varies quite a bit (Fig. 2A, triangles) but again shows no correlation with the enhanced convective intensity as  $N_a$  of  $UAP_{<50}$  increases. Analyses of profiles of the temperature, relative humidity (RH), and zonal U- and meridional V-components of the wind fields representative of the pre-storm environment also indicate that these environmental profiles do not correlate with an increase of updraft intensity as  $N_a$  of  $UAP_{<50}$  increases (fig. S3). In fact, our lowest- $N_a$  group exhibited higher RH at 2- to 5-km altitudes than did the higher- $N_a$  groups, which should have favored stronger convection and offset some aerosol effects. This means that the trend for enhanced updraft intensity with the increase of  $N_a$  counting  $UAP_{<50}$  should have potentially been more prominent if RH for the lowest- $N_a$  group is similar to those of the higher- $N_a$  groups. Although we cannot





and thermodynamical environments (33, 35). We examined traditional radiosonde thermodynamic forcing parameters such as the convective available potential energy (CAPE) and convective inhibition (CIN) before convection. The CAPE is very similar for these events (Fig. 2A, black circles) and is not strongly correlated with updraft intensity. Under similar CAPE conditions, CIN magnitudes should help to reveal how likely it is for DCCs to initiate and to determine what may be their relative intensities. CIN varies quite a bit (Fig. 2A, triangles) but again shows no correlation with the enhanced convective intensity as  $N_a$  of  $\text{UAP}_{<50}$  increases. Analyses of profiles of the temperature, relative humidity (RH), and zonal U- and meridional V-components of the wind fields representative of the pre-storm environment also indicate that these environmental profiles do not correlate with an increase of updraft intensity as  $N_a$  of  $\text{UAP}_{<50}$  increases (fig. S3). In fact, our lowest- $N_a$  group exhibited higher RH at 2- to 5-km altitudes than did the higher- $N_a$  groups, which should have favored stronger convection and offset some aerosol effects. This means that the trend for enhanced updraft intensity with the increase of  $N_a$  counting  $\text{UAP}_{<50}$  should have potentially been more prominent if RH for the lowest- $N_a$  group is similar to those of the higher- $N_a$  groups. Although we cannot



and thermodynamical environments (33, 35). We examined traditional radiosonde thermodynamic forcing parameters such as the convective available potential energy (CAPE) and convective inhibition (CIN) before convection. The CAPE is very similar for these events (Fig. 2A, black circles) and is not strongly correlated with updraft intensity. Under similar CAPE conditions, CIN magnitudes should help to reveal how likely it is for DCCs to initiate and to determine what may be their relative intensities. CIN varies quite a bit (Fig. 2A, triangles) but again shows no correlation with the enhanced convective intensity as  $N_a$  of  $UAP_{<50}$  increases. Analyses of profiles of the temperature, relative humidity (RH), and zonal U- and meridional V-components of the wind fields representative of the pre-storm environment also indicate that these environmental profiles do not correlate with an increase of updraft intensity as  $N_a$  of  $UAP_{<50}$  increases (Fig. S2). In fact, our lowest  $N_a$

those of the higher- $N_a$  groups. Although we cannot guarantee that RWP observations captured the representative updraft cores for every single event, these analyses do not show any covariation of aerosols with dynamics and thermodynamics for these locally occurring systems. This provides clear evidence that the enhanced convective intensity seen with the increase in  $N_a$  of  $UAP_{<50}$  is not solely controlled by factors other than  $UAP_{<50}$ .

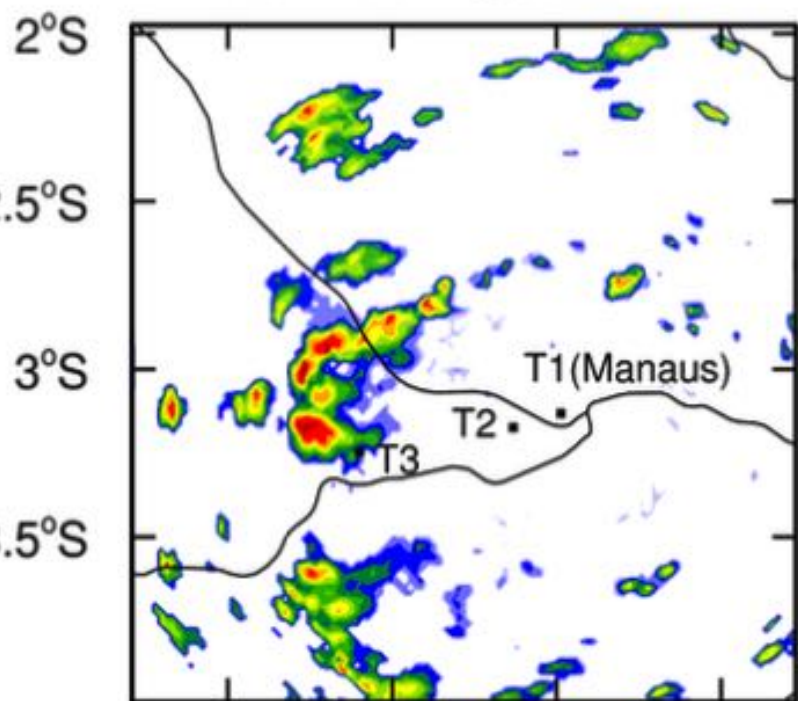
# Modeling

- To understand the physical processes and mechanisms responsible for the observed intensification of updrafts by UAP<50, ....
- we conducted model simulations at a cloud-resolving scale of 0.5 km for a typical wet season convective event, as on 17 March.
- We used detailed spectral-bin microphysics coupled with the WRF model

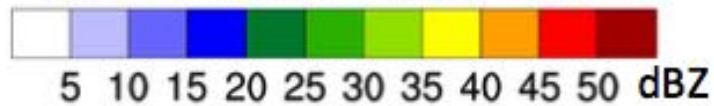
A

## SIPAM

2014-03-17\_18:23:14



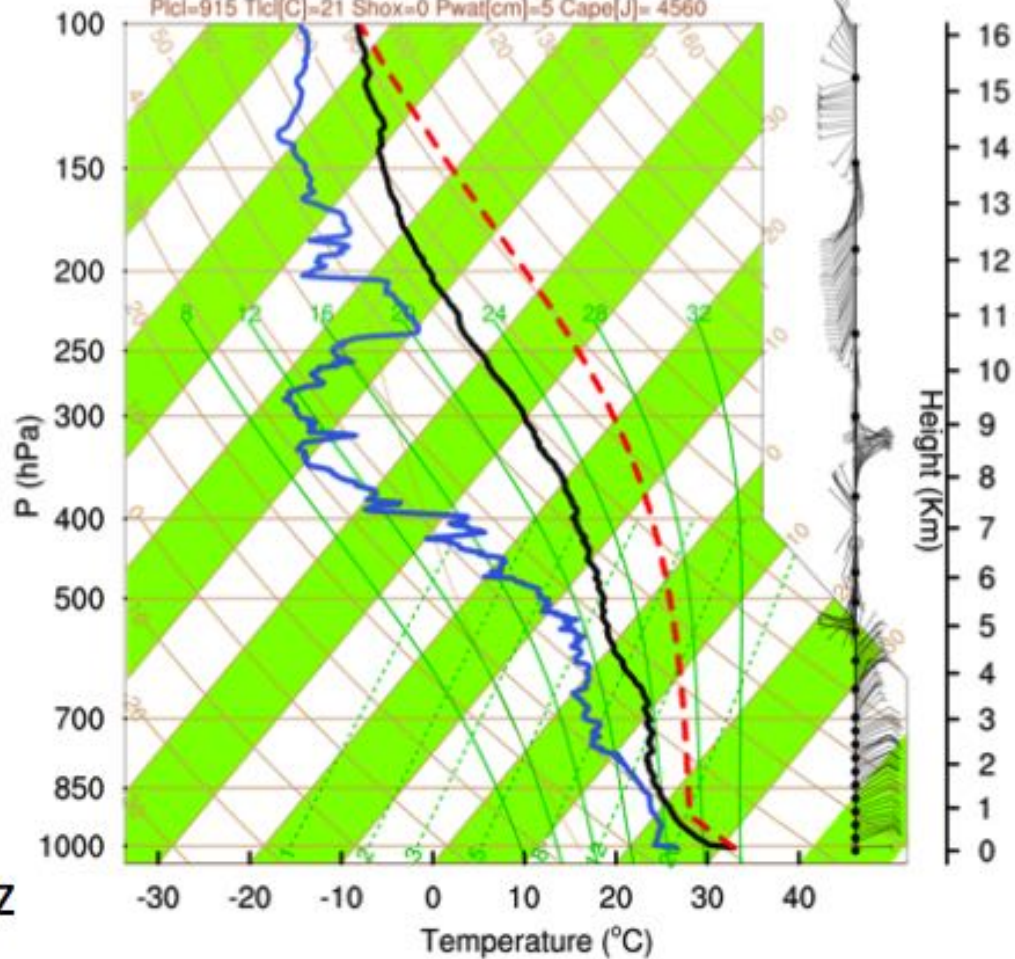
61°W 60.5°W 60°W 59.5°W

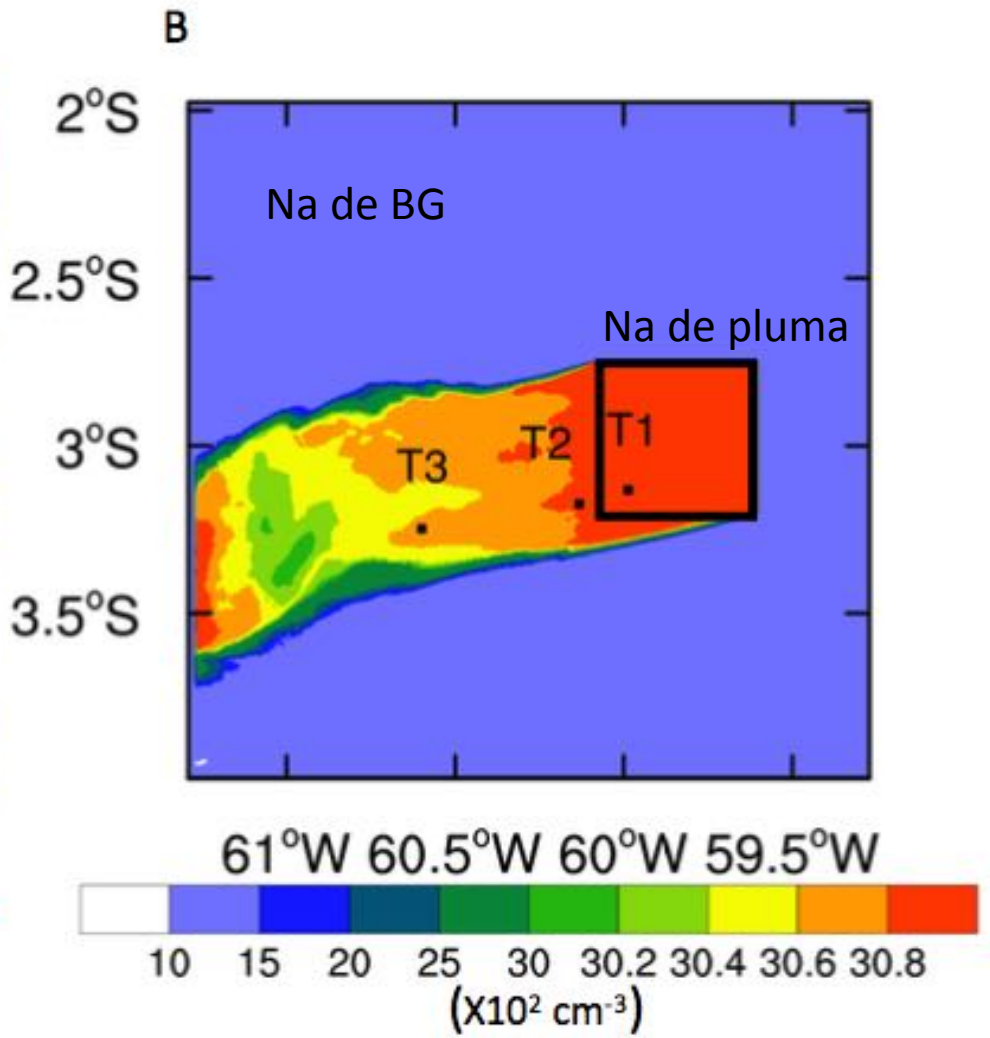
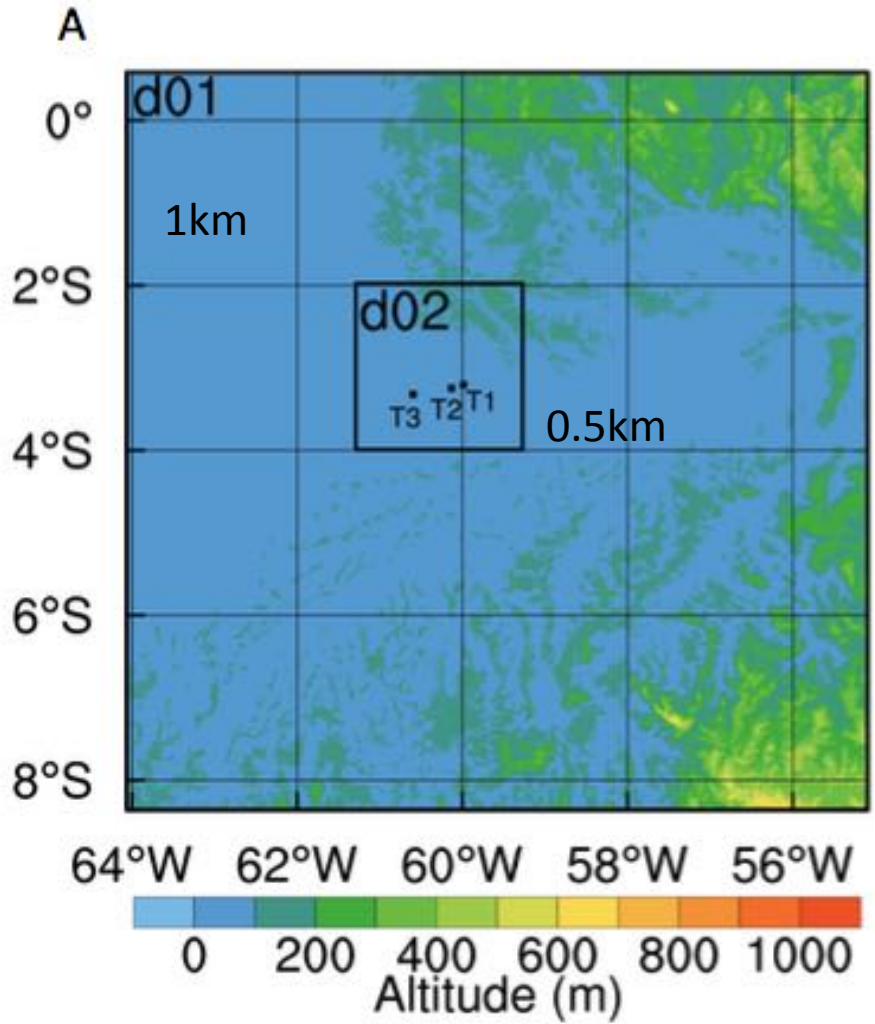


B

Sounding: 2014-03-17\_14:20:00 at T3

Pfc1=915 Tfc1[C]=21 Shox=0 Pwat[cm]=5 Cape[J]= 4560



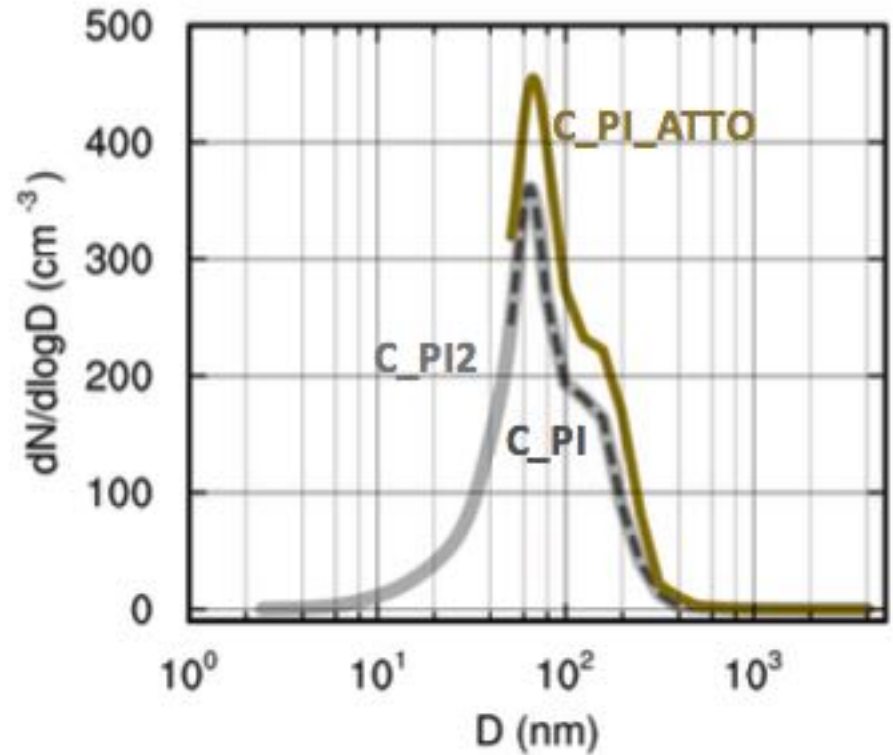
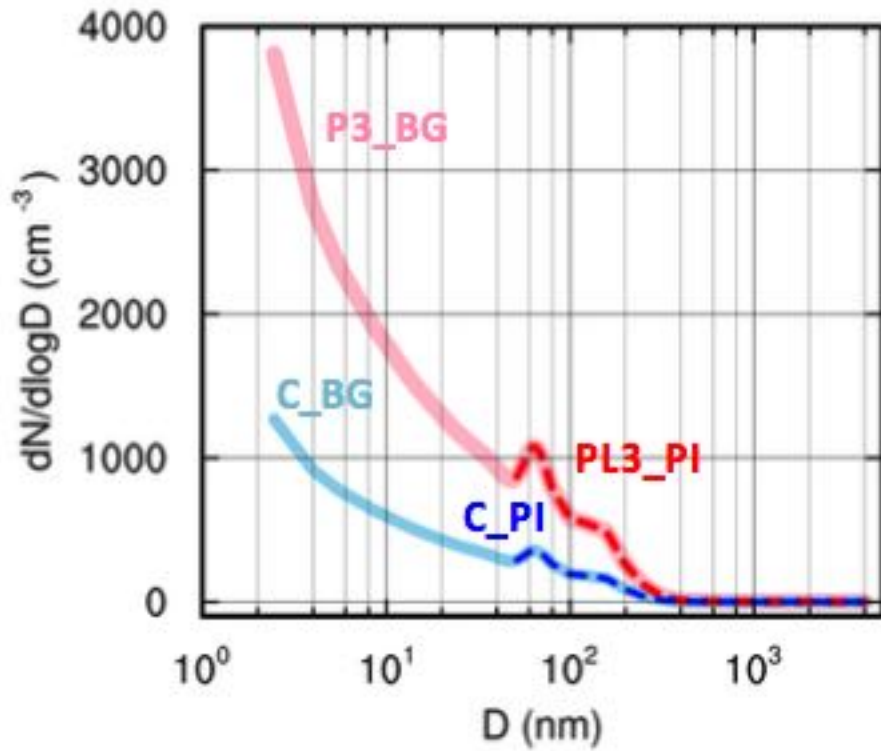


# Configuration

- Soil moisture from CPTec/INPE, 0.25 degree
- The surface albedo, vegetation, and green fraction from Alvalá/Prodis
- Domain 01, 1km, 1000×1000 // domain #2, 0.5 km, 450×450
- 51 vertical levels up to 50 hPa.
- Noah land surface scheme,
- RRTMG for SW and LW
- Yonsei PBL
- NO Cumulus parameterization
- Simulations over d02 using the “ndown” approach.
- Forcing: NCEP/FNL at 1-deg and 6-h
- 36h simulations initiated at 12:00 UTC on 16 March, output = 5-min
  
- We purposely avoided using grey-zone resolutions
- To buffer the “jump” from 1-deg, used 30 points boundaries in d01.

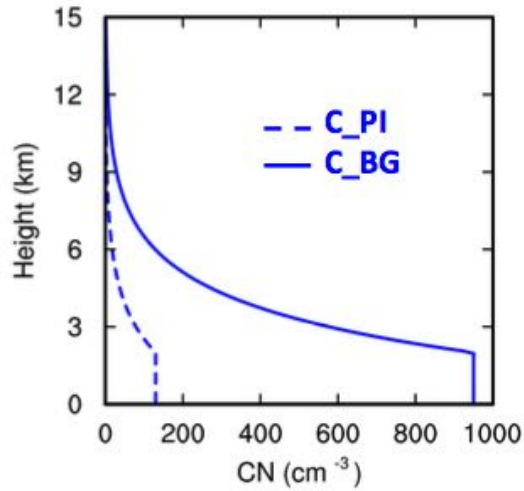
Simulation	Acronym	Size distribution	Vertical distribution	Hygroscopicity ( $\kappa$ )	$N_a$ of domain (per cubic centimeter)		$N_a$ of Manaus pollution plume (per cubic centimeter)	
					CCN <sub>&gt;50</sub>	UAP <sub>&lt;50</sub>	CCN <sub>&gt;50</sub>	UAP <sub>&lt;50</sub>
Manaus regional background with pollution plume	P3_BG	Power law + peaked	Exponential decrease	0.12	130	820	390	2460
Manaus regional background	C_BG	Power law + peaked	Exponential decrease	0.12	130	820	N/A	N/A
PI condition without UAP <sub>&lt;50</sub>	C_PI	Peaked	Exponential decrease	0.12	130	0	N/A	N/A
Sensitivity test for P3_BG without UAP <sub>&lt;50</sub>	PL3_PI	Peaked	Exponential decrease	0.12	130	0	390	0
Sensitivity test for VD based on C_BG	C_BG_VD	Power law + peaked	Upper-level peak	0.12	130	820	N/A	N/A
Sensitivity test for VD based on C_PI	C_PI_VD	Peaked	Upper-level peak	0.12	130	0	N/A	N/A
Sensitivity test for SD based on P3_BG	P3_BG_SD	Peaked	Exponential decrease	0.12	450	3350	1350	10,050
Sensitivity test for SD based on C_BG	C_BG_SD	Peaked	Exponential decrease	0.12	450	3350	N/A	N/A
Sensitivity test for SD based on C_PI	C_PI_SD	Peaked	Exponential decrease	0.12	450	0	N/A	N/A
PI condition with UAP <sub>&lt;50</sub>	C_PI2	Peaked	Exponential decrease	0.12	130	60	N/A	N/A
Sensitivity test for C_PI with mean ATTO	C_PI_ATTO	Peaked	Exponential decrease	0.12	200	0	N/A	N/A
Sensitivity test for C_BG with CCN <sub>&gt;50</sub> from mean ATTO	C_BG_ATTO	Peaked	Exponential decrease	0.12	200	820	N/A	N/A

# Size distribution

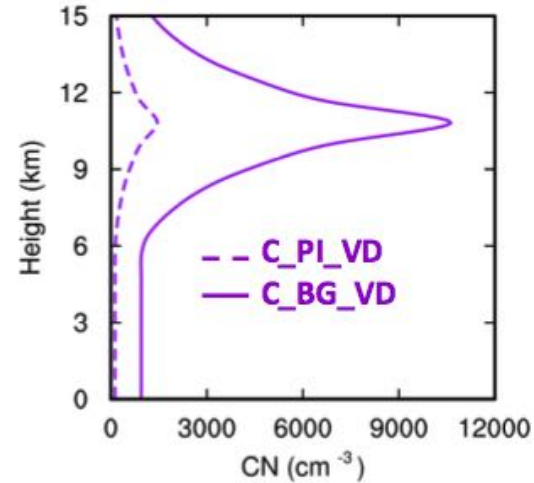


# Vertical distribution

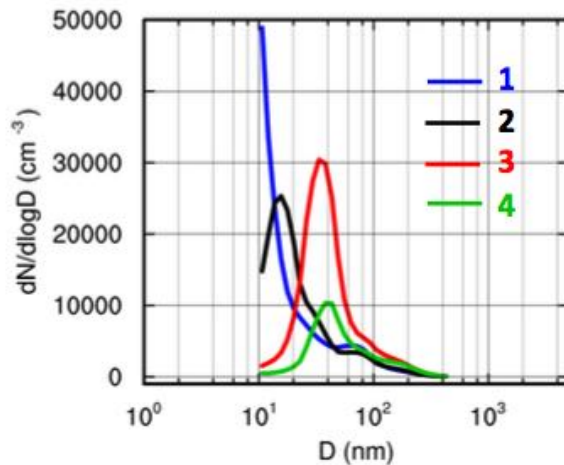
A Original VD



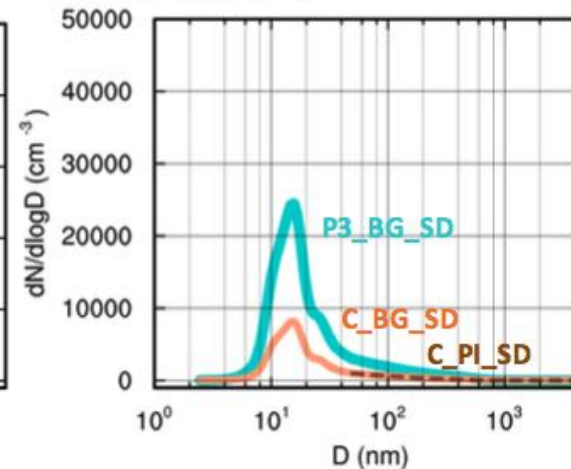
B Tested VD



C Observed

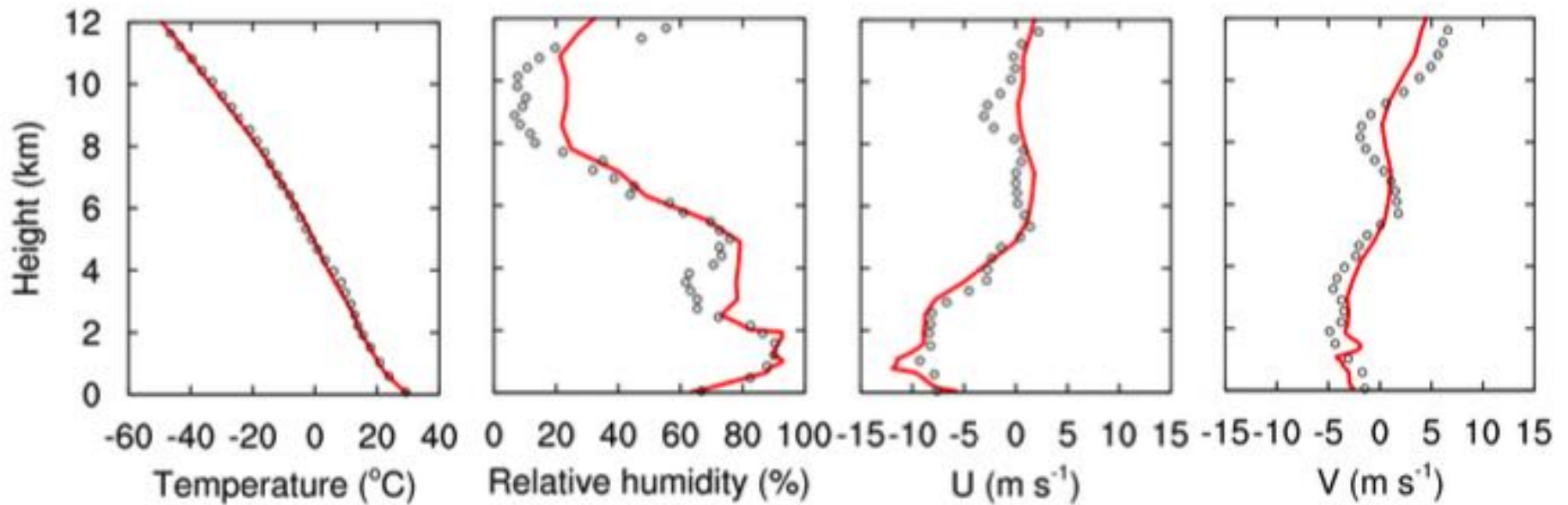


D Tested SD



# Model results - check

Fig. S7. Comparison of the temperature, RH, U- and V-winds from the sounding data at 14:20 UTC at the T3 site (circle) with those from the same time and location in P3\_BG (red).



# Check 2

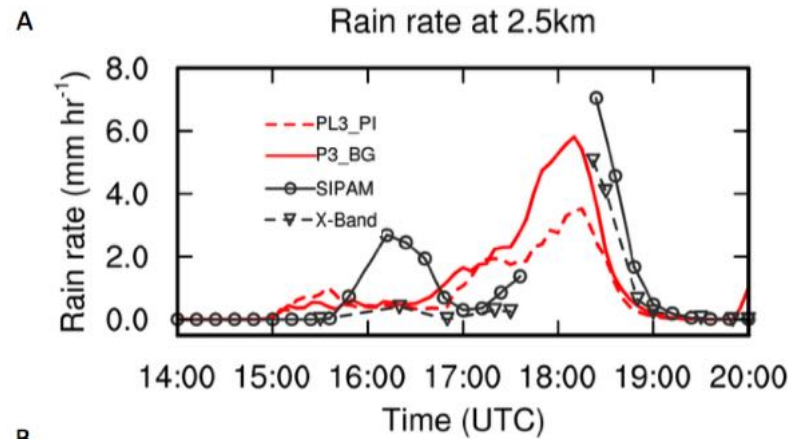
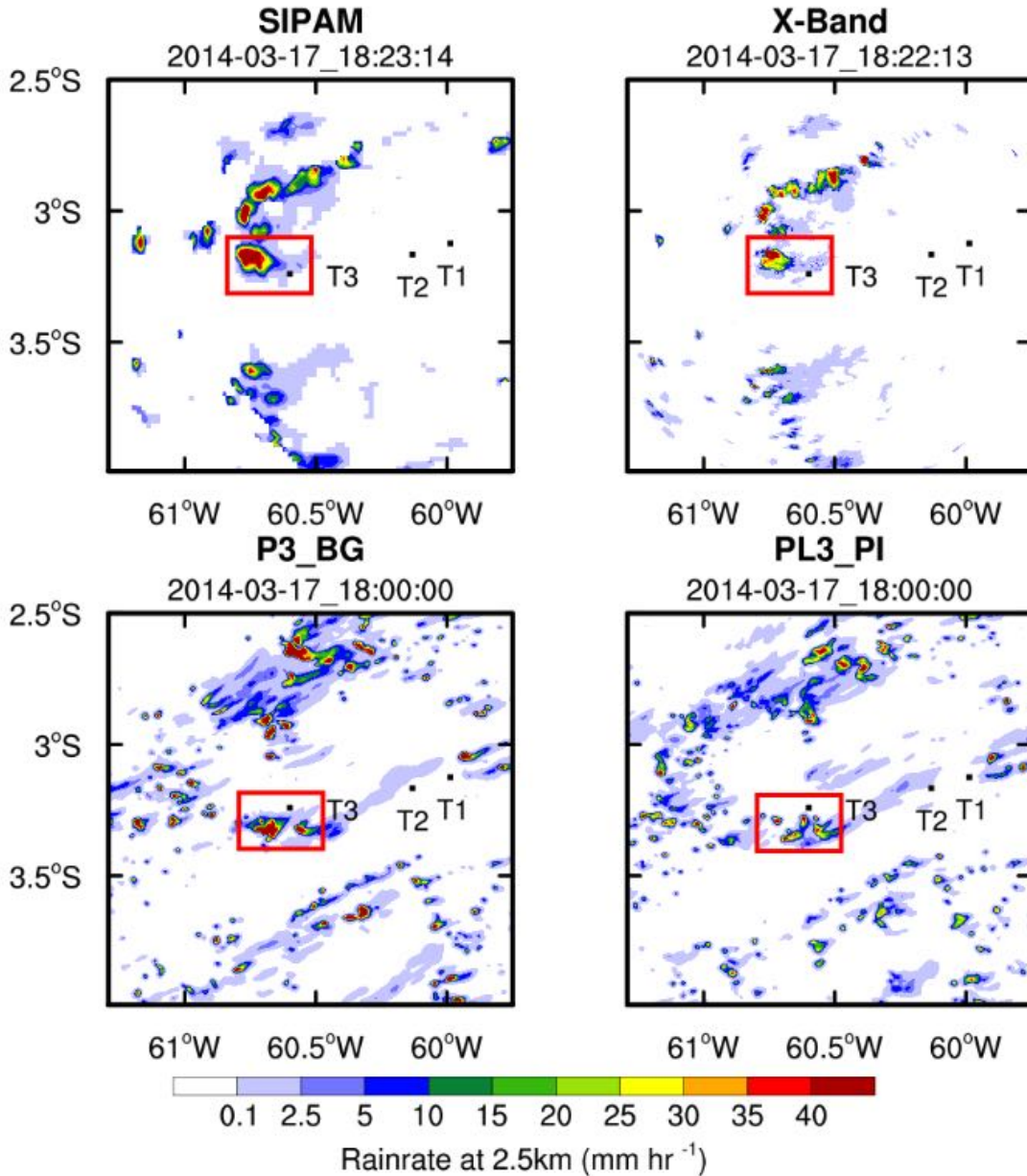
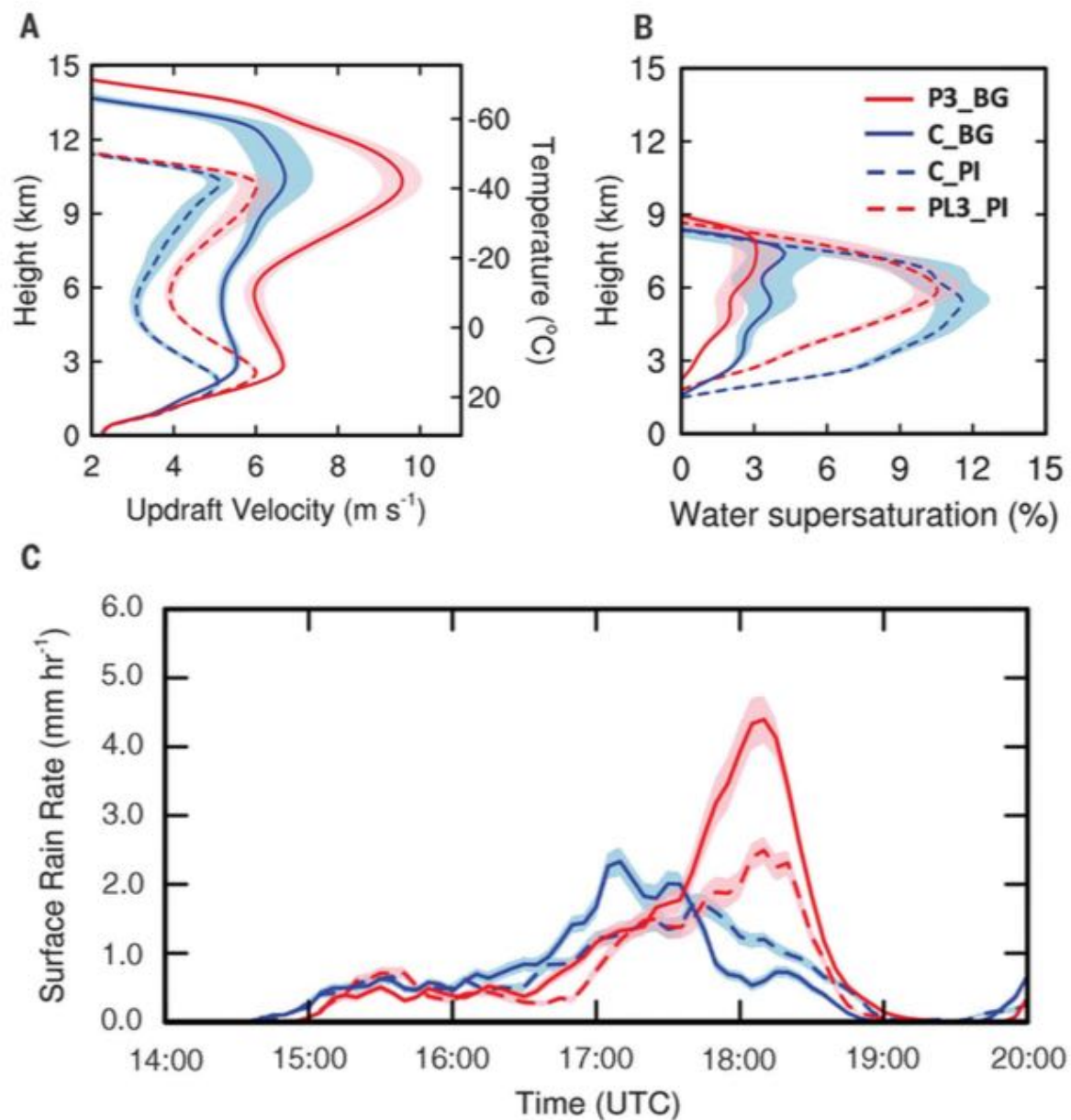


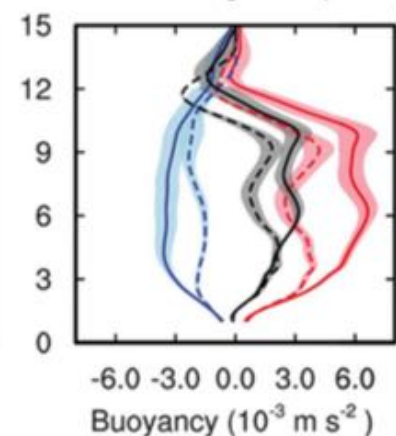
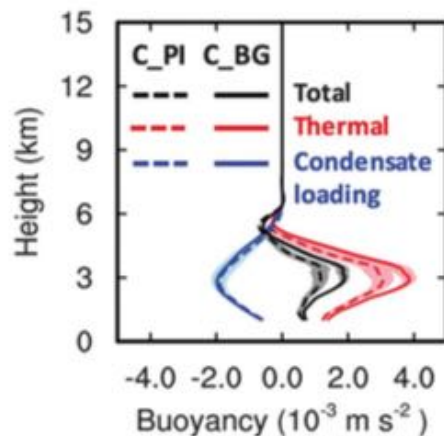
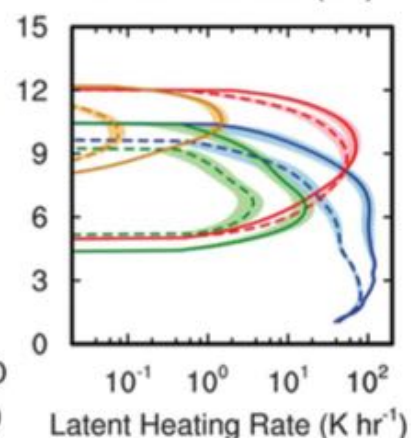
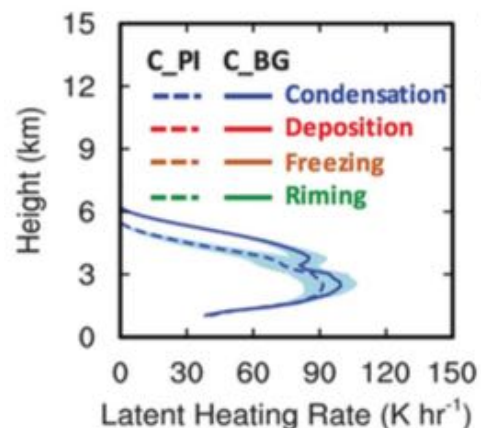
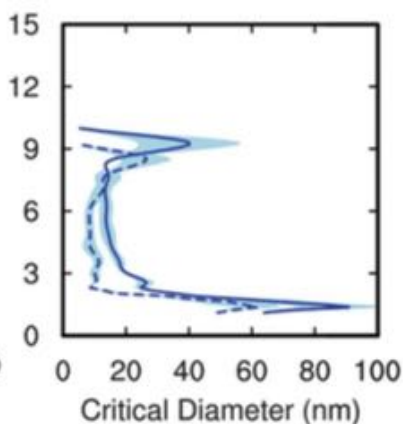
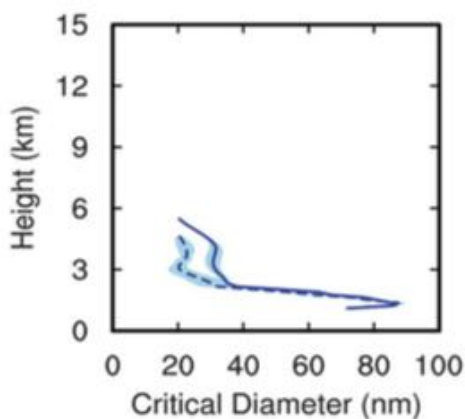
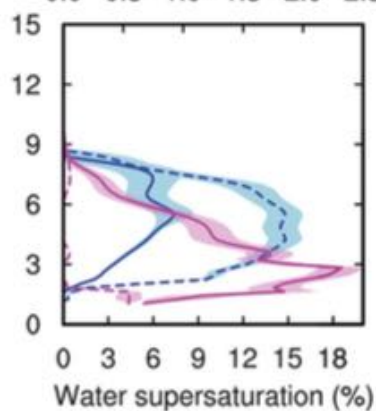
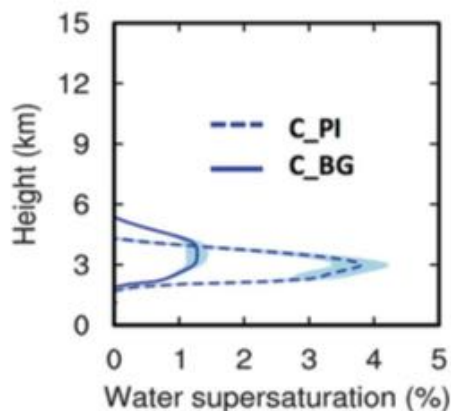
**Fig. 3. Simulated aerosol effects on the DCCs.**

(A and B) Vertical profiles of updraft velocity  $w$  (A) and water supersaturation (B) averaged over the top 10 percentiles (i.e., 90th to 100th) for the updrafts with  $w > 2 \text{ m s}^{-1}$  during 1400–1900 UTC from the convective clouds around the T3 site (red box in fig. S8). (C) Time series of mean surface rain rate averaged over the red box area from simulations of C\_PI (blue dashed curve), C\_BG (blue solid curve), PL3\_PI (red dashed curve), and P3\_BG (red solid curve). The right-side y axis in (A) shows the temperature profile. The convective clouds over T3 were chosen for analysis because they are affected by the Manaus pollution plume in P3\_BG and evaluated by observations as shown in figs. S7 to S9. Comparisons with radar-retrieved rain rates at 2.5-km altitude are shown in figs. S8 and S9A. Shaded areas represent the standard error of the data.



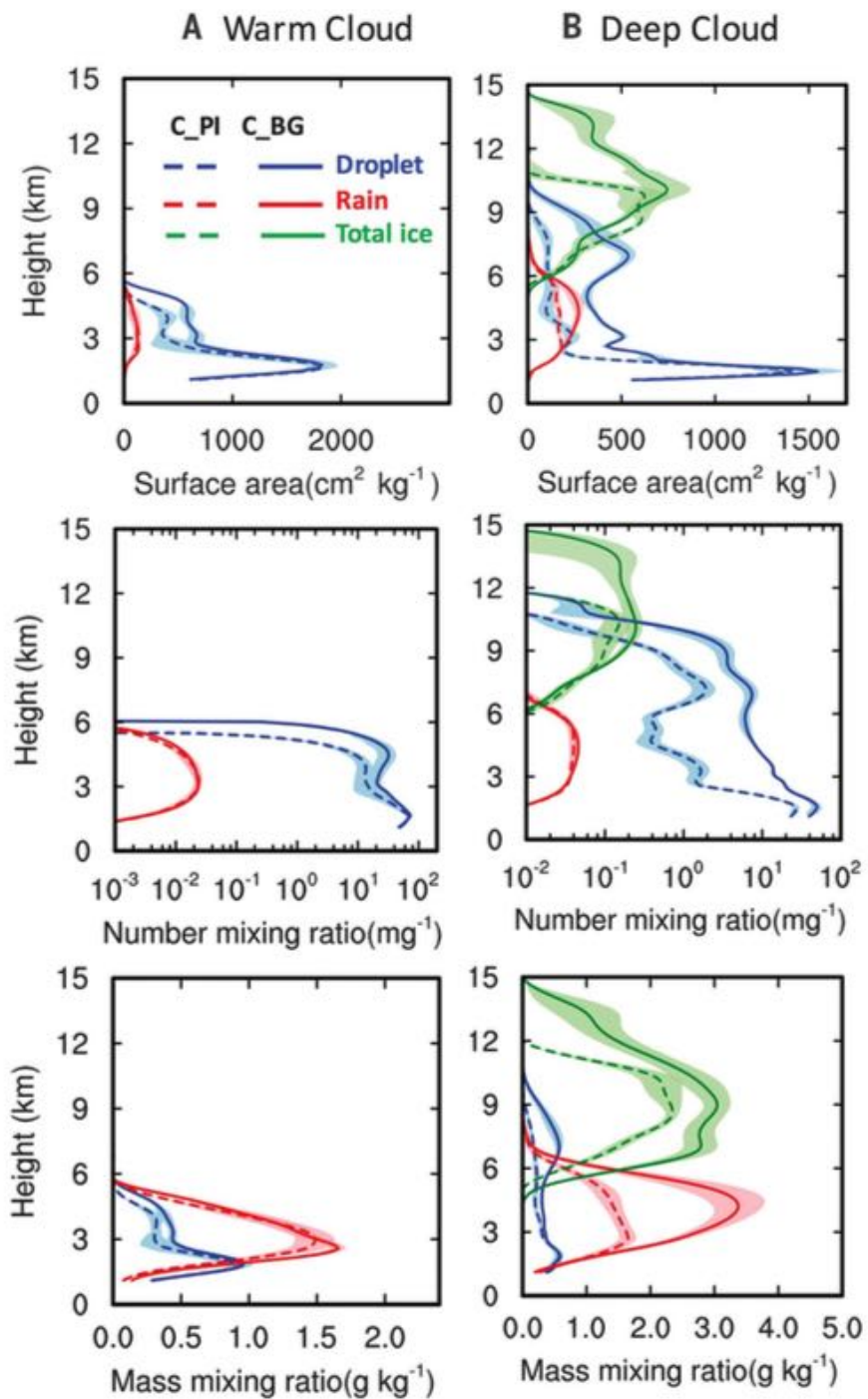
**A Warm Cloud****B Deep Cloud**Drop nucleation rate ( $\text{mg}^{-1} \text{s}^{-1}$ )

0.0 0.5 1.0 1.5 2.0 2.5



variations. The values for the warm cloud are averaged over the top 10 percentiles (i.e., 90th to 100th) of the updrafts with  $w > 1 \text{ m s}^{-1}$  from a 30-min duration after the warm rain starts and the rain rate exceeds  $0.5 \text{ mm hour}^{-1}$  for the convective clouds in the red box in fig. S8.

The values for the deep cloud are averaged over the top 10 percentiles (i.e., 90th to 100th) of the updrafts with  $w > 2 \text{ m s}^{-1}$  from a 30-min duration with 15 min before and after the strongest convection. Therefore,



# Paper conclusions

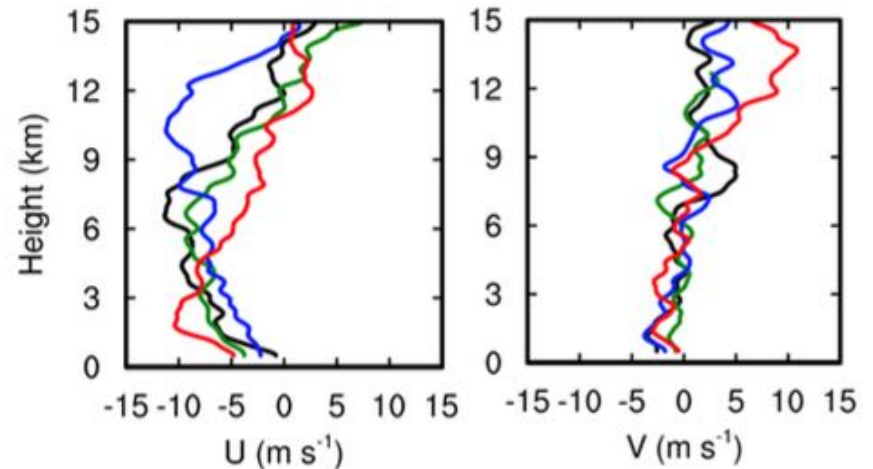
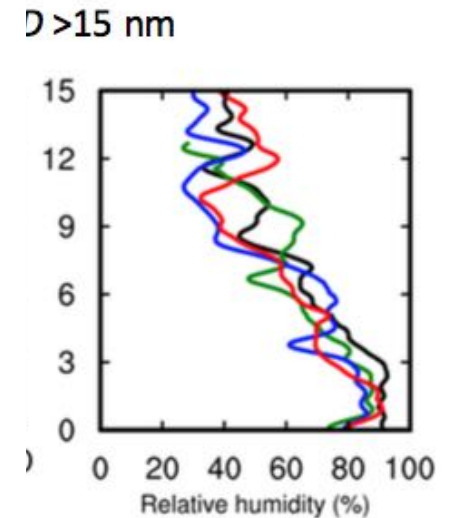
- The retrieved updraft velocity from RWP has allowed us to directly examine and constrain aerosol impacts on updraft intensity for DCCs occurring in a **similar dynamic and thermodynamic** (...), revealing (...) convective updraft and precipitation enhancements by UAP<50 from the Manaus pollution plume.
- The physical mechanism (...) stems from the strong capacity of these DCCs in activating UAP<50 that usually have a much higher number concentration than CCN>50
- The subsequent condensational growth of an additional number of droplets (...) lowers SS, liberating a large amount of additional LH at the low and middle levels of DCCs and considerably enhancing updraft strength.

# Conclusions

- This “warm-phase invigoration” has much stronger effects than the “cold-phase invigoration” previously proposed.
- UAP<50 increase the rainwater amount mainly through enhanced accretion of added cloud droplets and added graupel melting.
- UAP<50 do not affect the timing of precipitation because UAP<50 can be activated to form additional cloud droplets only after warm rain begins.
- In contrast, CCN>50 suppress and delay warm rain and then delay peak precipitation.

# My critics

- Only 17 events / in 4 classes
  - why not 2015 too?
- Thermodyn. not the same
  - 1d simulation MicPhys?



# My critics

- Only 17 events / in 4 classes
  - why not 2015 too?
- Thermodyn. not the same
  - 1d simulation MicPhys?
- Simulation of 1 golden case

# My critics

- Only 17 events / in 4 classes
  - why not 2015 too?
- Thermodyn. not the same
  - 1d simulation MicPhys?
- Simulation of 1 golden case
- Jump 1deg => 1km
  - Proof that 30grid margin is enough?



## Lateral boundary conditions for limited area models

Terry Davies\*

MetOffice@Reading, Reading, UK

\*Correspondence to: T. Davies, MetOffice@Reading, Meteorology Building, University of Reading, Reading RG6 7BE, UK. E-mail: terry.davies@metoffice.gov.uk

### (a) Differences in resolution

The effects of differences in spatial resolution at boundaries are mainly evident where information is outgoing and where scales below the smallest scales represented by the LBCs have been generated within the LAM. LBCs only contain scales represented by the driving model and near inflow boundaries the LAM will also tend to contain the same scales since it takes time to generate the smaller scales (see example later). However, at outflow boundaries the LAM will contain smaller scales which cannot be matched by the LBCs. These scales need to be damped by the blending to reduce the effects of the mismatch (Temam and Tribbia, 2003). It is possible that the LAM can also mismatch scales

the UM LBC strategy for a case with a deep depression crossing Scotland. Other cases have been run with similar impacts. The results above demonstrate that the UM LBC formulation works well and that the LBC error is only a small fraction of the overall error. The main design feature of the LBC algorithm is that it is effectively transparent for no difference in resolution between the LAM and LBCs when LBCs are supplied every time step. Even when the grid-length ratio between the LBCs and LAM is 4:1 LBC errors are mostly confined to the outflow boundaries and inflow boundaries are effectively transparent, i.e. all information that enters the boundaries is used.

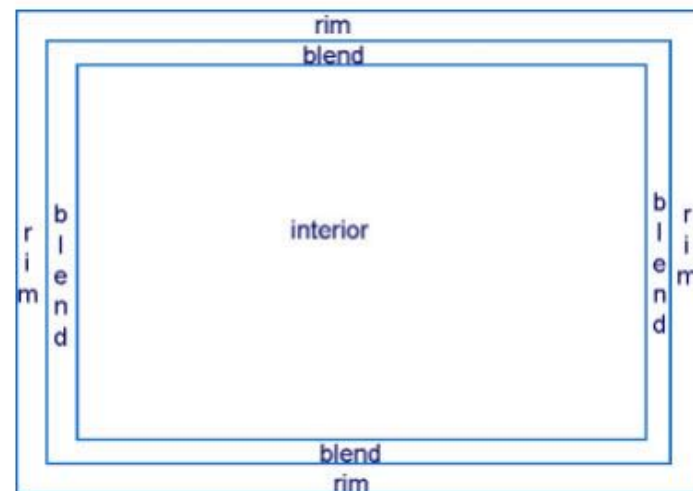
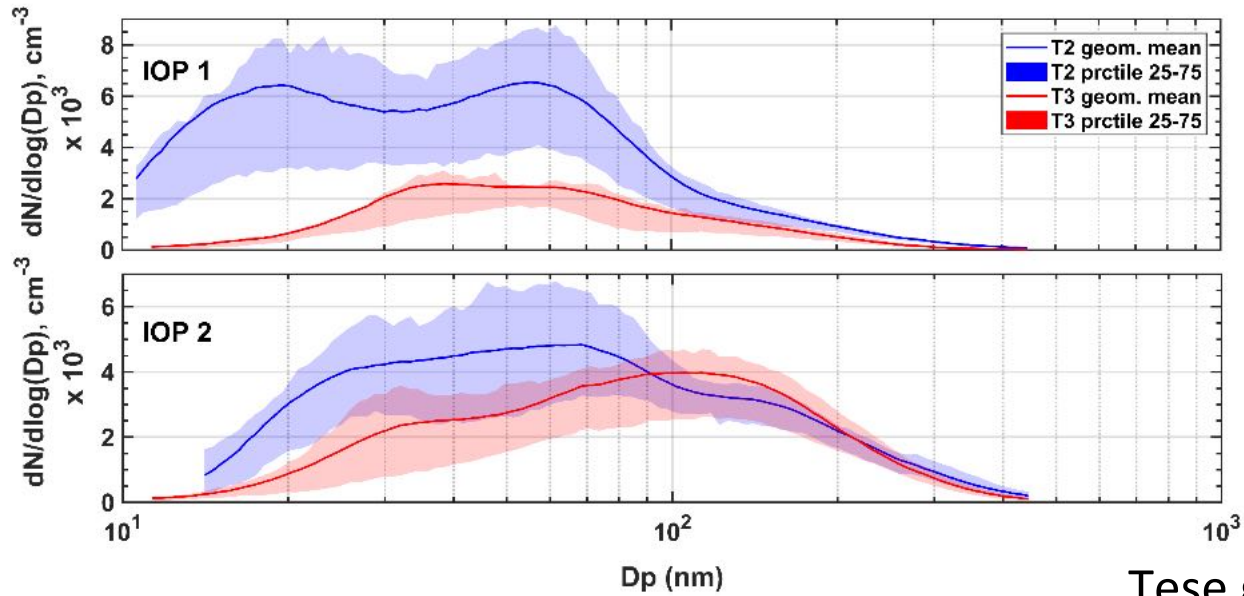
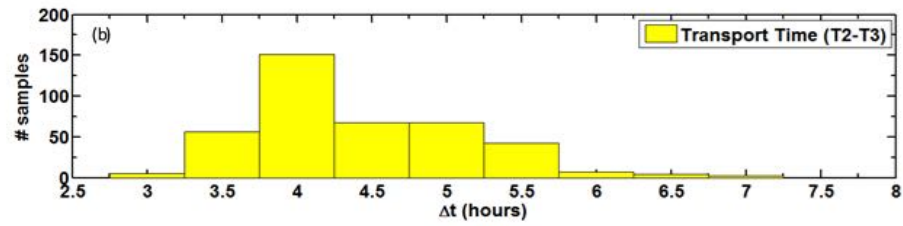
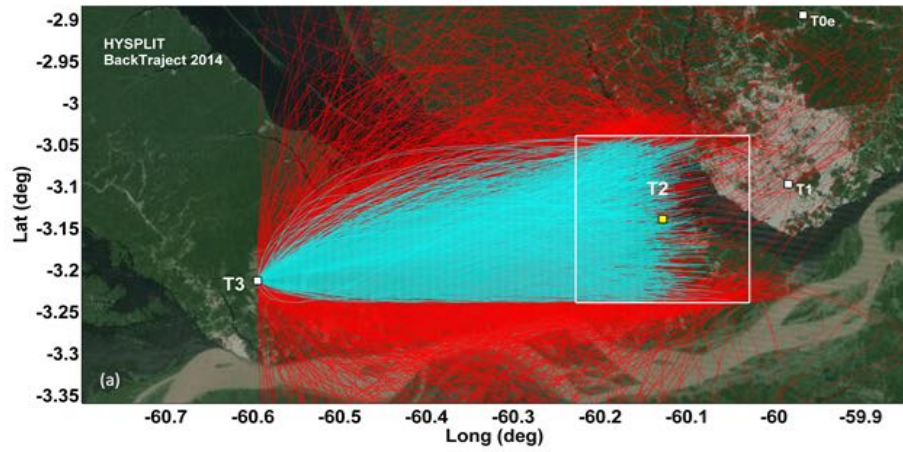


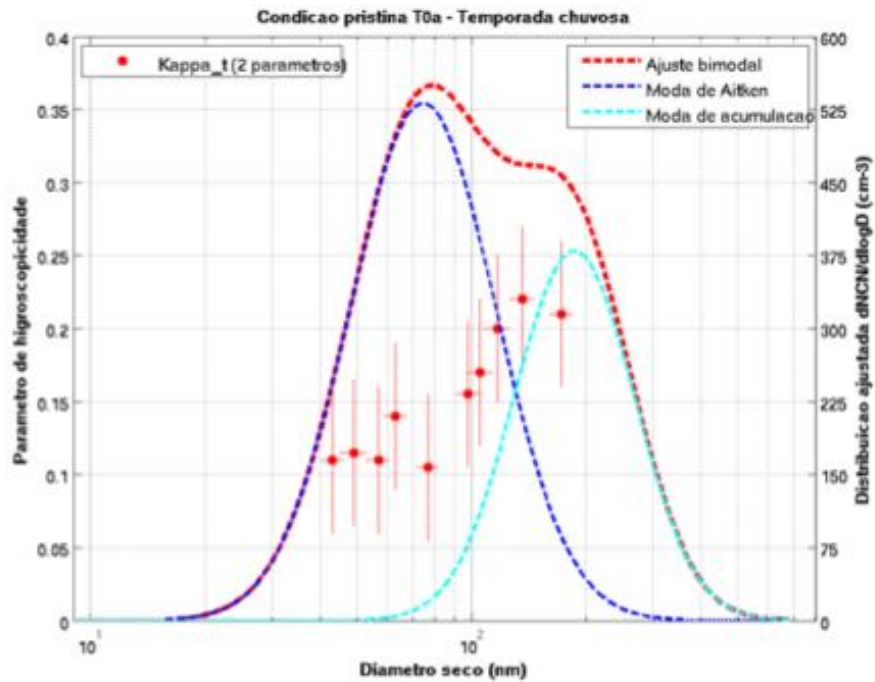
Figure 1. Regions of an LAM domain. See text for an explanation. This figure is available in colour online at [wileyonlinelibrary.com/journal/qj](http://wileyonlinelibrary.com/journal/qj)

the nearest integer greater than the maximum Courant number plus 2 fewer than the order of interpolation used in the semi-Lagrangian scheme for obtaining departure point values. Thus, for a maximum Courant number of 4 and using cubic interpolation, 5 points are needed at inflow lateral boundaries to provide boundary conditions for semi-Lagrangian advection.

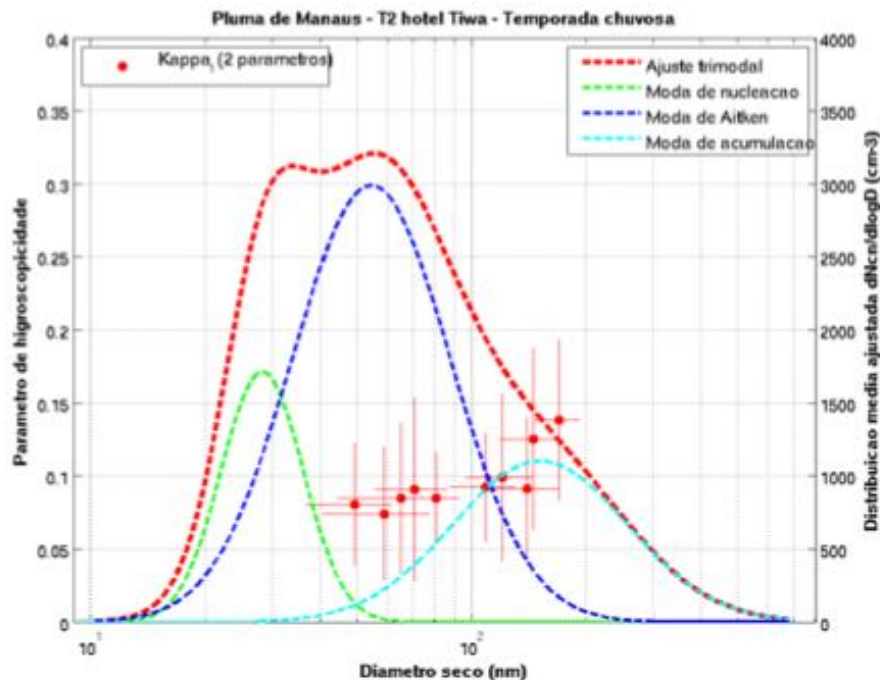
# My critics

- Only 17 events / in 4 classes
  - why not 2015 too?
- Thermodyn. not the same
  - 1d simulation MicPhys?
- Simulation of 1 golden case
- Jump 1deg => 1km
  - Proof that 30grid margin is enough?
- Size distributions (no -Chem)
  - Changing Na should change size and kappa too

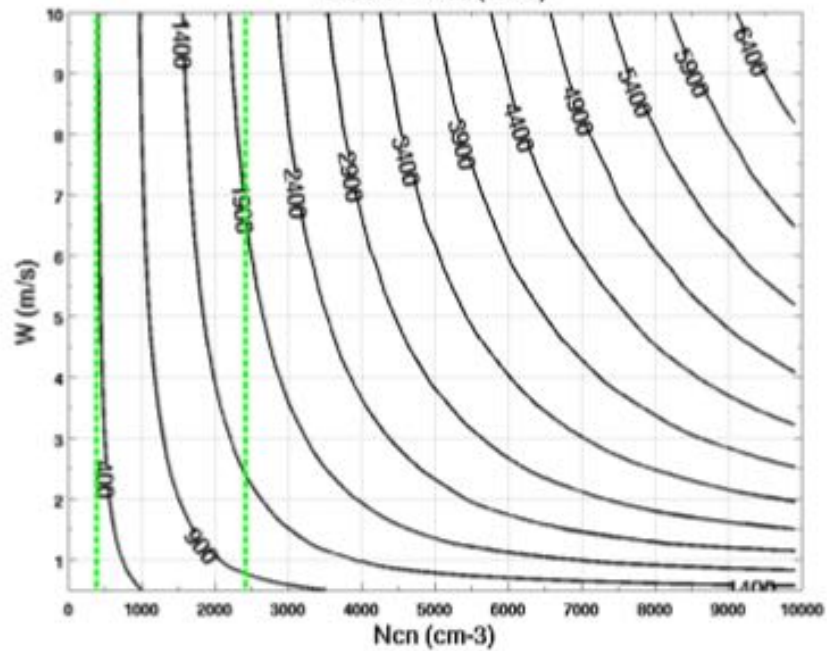




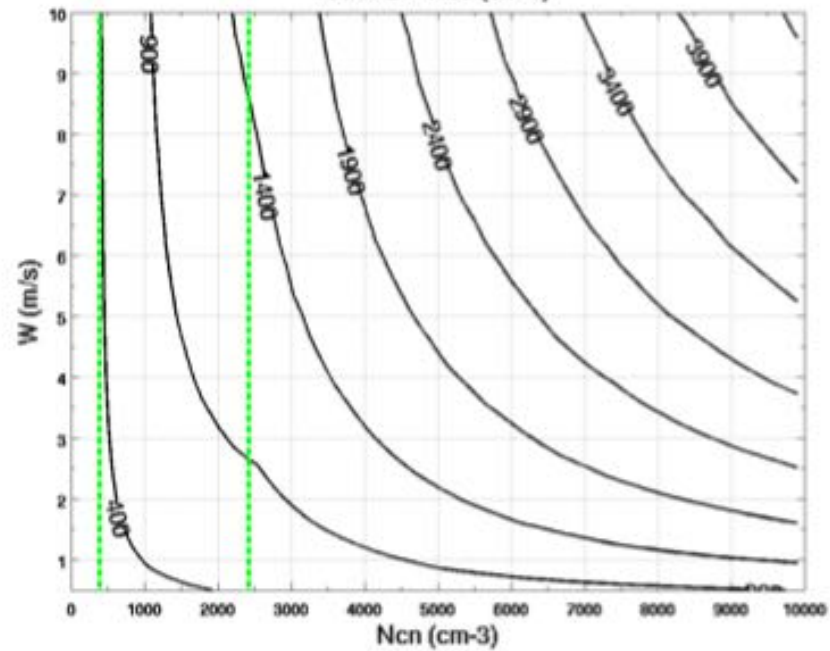
- Caso 1: SD, k
- Caso 2: SD(Na), k
- Caso 3: SD(Na), k(Na)
- Caso 4: SD(Na), k(D, Na)



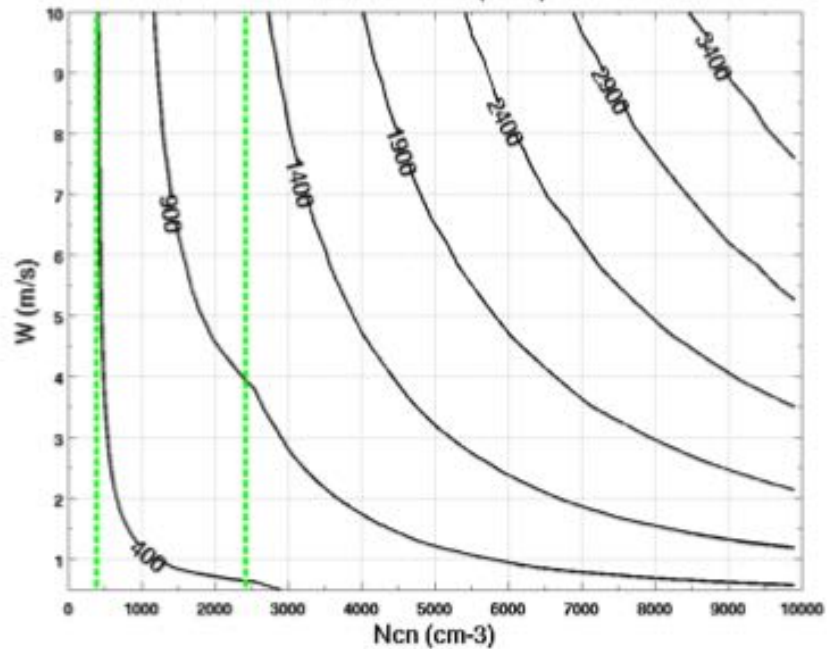
Caso 1 - Ncd (cm-3)



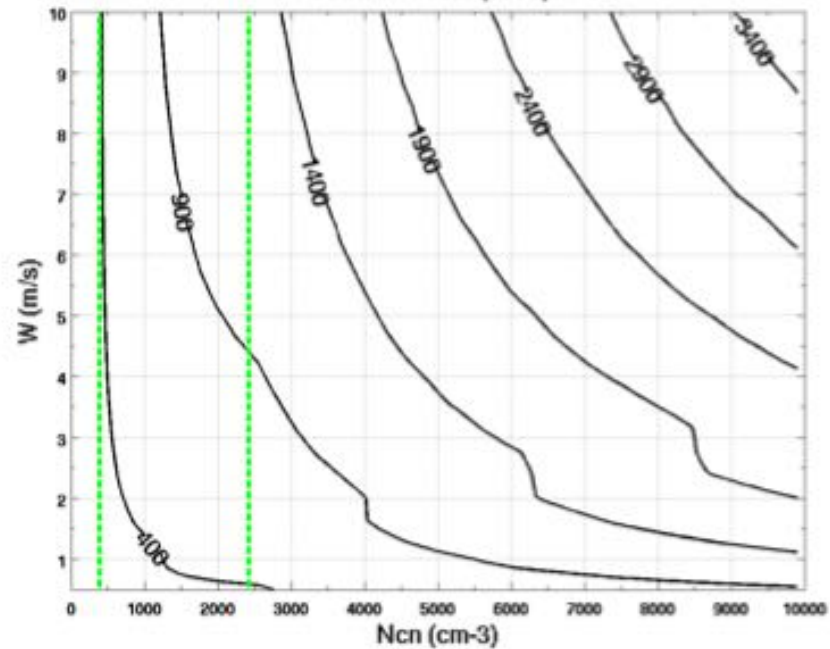
Caso 2 - Ncd (cm-3)



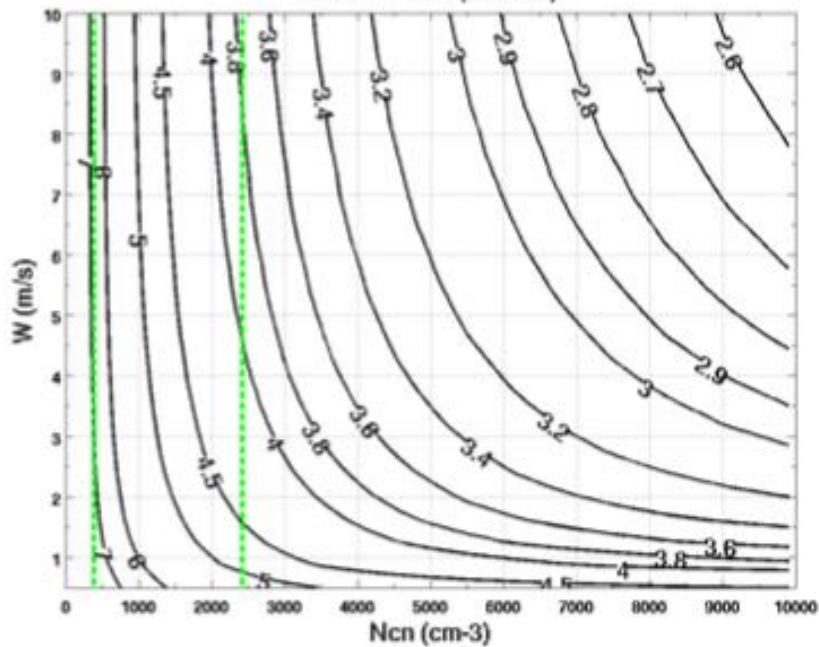
Caso 3 - Ncd (cm-3)



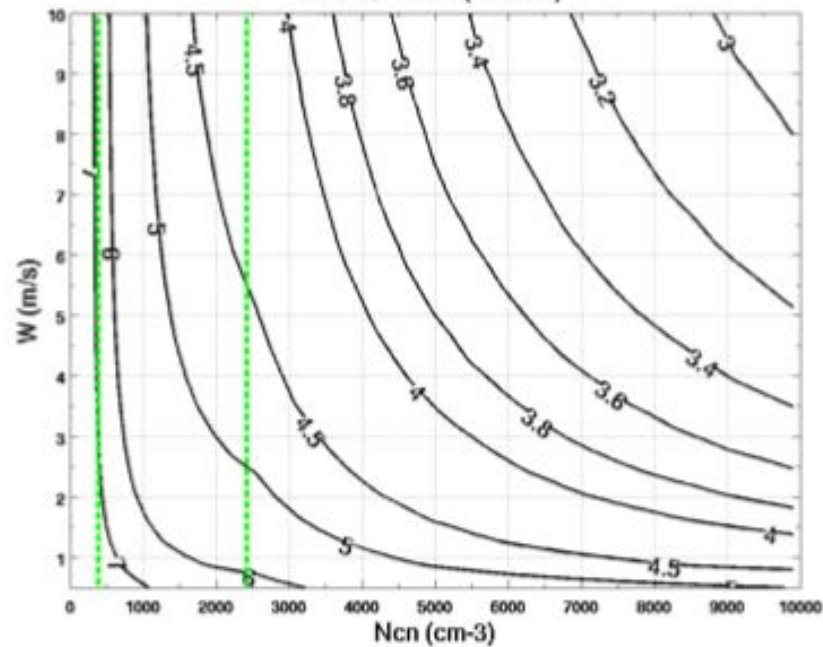
Caso 4 - Ncd (cm-3)



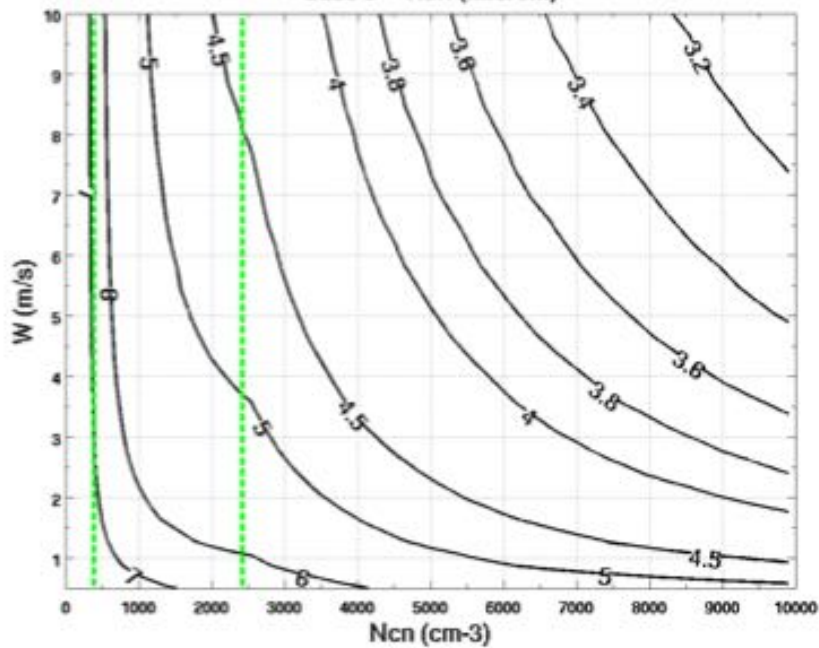
Caso 1 - Reff (microm)



Caso 2 - Reff (microm)



Caso 3 - Reff (microm)



Caso 4 - Reff (microm)

